Investigation of allele-specific expression in citrus hybrids reveals the association between siRNA-mediated de novo methylation and high expression in citrus genomes

Diop Khadidiatou[1], Bonnin Marie[1,2,3], Gibert Anaïs[1], Christel Llauro[1], Yann Froelicher[4], Hufnagel Barbara[5]*, Picault Nathalie[1]*, Pontvianne Frédéric[1]*

[1]CNRS/UPVD, Plant Genome and Development (LGDP), Perpignan, 66100, France
[2]CNRS, Equipe d'Adaptation des végétaux aux changements globaux, Projet Ressources Naturelles, UMR 6134 SPE, Univ de Corse, Corsica, France.
[3]UMR AGAP Institut, Univ Montpellier, CIRAD, INRAE, Institut Agro, Montpellier, France
[4]CIRAD, UMR AGAP Institut, F- 20230 San Giuliano, France. UMR AGAP Institut, Univ Montpellier, CIRAD, INRAE, Institut Agro, Montpellier, France.
[5]CIRAD, UMR AGAP Institut, F-97170 Petit-Bourg, Guadeloupe, France. UMR AGAP Institut, Univ Montpellier, CIRAD, INRAE, Institut Agro, Montpellier, France.

*co-corresponding authors
frederic.pontvianne@cnrs.fr, nathalie.picault@univ-perp.fr, barbara.hufnagel@cirad.fr,

Authors Orcid ID:
Khadidiatou Diop: 0009-0001-2255-7489
Frederic Pontvianne: 0000-0002-2913-4104
Nathalie Picault: 0000-0003-2770-9688
Barbara Hufnagel: 0000-0002-3515-2122
Marie Bonnin: 0000-0002-1533-5052

Abstract

DNA methylation plays a central role in the regulation of gene expression. In plants, methylation occurs in the CG, CHG and CHH contexts, *via* distinct DNA methyltransferases including MET1, CMT3 and the RNA-directed DNA Methylation (RdDM) pathway *via* DRM2. In interspecific hybrids, these epigenetic mechanisms are confronted to a mixed small RNA population and two subgenomes harbouring specific methylation patterns, therefore generating unique expression profiles. The aim of this work was to understand these regulations by analysing gene expression, DNA methylation and small RNAs in a Citrus hybrid resulting from the cross between *C. reticulata* (mandarin) and *C. australasica* (finger lime). Haplotype-resolved subgenomes assembly identified hundreds of allele-specifically expressed genes. Asymmetric reprogramming of methylation was observed, in particular an

increase in CHH in *C. australasica* haplotype. Surprisingly, CHH methylation, usually associated with gene silencing, was correlated here with increased expression, but also 24nt small RNA populations at their promoter regions. Similar analyses of the parental lines and other citrus species suggest the correlation between CHH methylation-enriched promoter and high expression level is not due to the hybridization, but seem to be generally true for all citrus. These observations suggest that, in citrus fruit, RdDM could activate transcription. This work also provides a full pipeline to analyse the expression profiles and DNA methylation in complex hybrids, which could be crucial for anticipating varieties resistant to diseases and the current threats affecting citriculture such as the Huanglongbing disease.

INTRODUCTION

Citrus fruits (*Citrus spp*.) are among the most economically and culturally significant fruit crops worldwide, with global production estimated at approximately 140–146 million tons annually (Mukhametzyanov et al., 2024). Their exceptional phenotypic diversity in fruit size, colour, flavour, essential oil composition, and nutritional value originates from a limited number of sexually compatible ancestral taxa - *C. medica*, *C. maxima*, *C. reticulata*, *C. micrantha*, and *C. cavaleriei* - whose interspecific hybridizations, followed by clonal propagation *via* apomixis and grafting, gave rise to the multitude of cultivated varieties ((Wu et al. 2018);(Ollitrault et al. 2020);(Curk et al. 2022)). While most commercial cultivars derive from combinations of these Asian ancestral taxa, recent phylogenomic analyses have led to the integration of formerly distinct genera such as *Microcitrus* and *Eremocitrus* into the genus *Citrus* ((Wu et al. 2018);(Curk et al. 2022)). These Oceanian lineages, including *C. australasica*, are genetically more distant from the Asian citrus gene pool, yet remain largely unused in modern breeding programs despite their potential to introduce novel adaptive traits (Nakandala et al. 2023).

Modern citriculture now faces an alarming convergence of challenges that threaten both productivity and sustainability. Among these, Huanglongbing (HLB), caused by *Candidatus Liberibacter spp*. and vectored by psyllids, has devastated citrus production in major growing regions, including Brazil, the United States, and China ((Costa et al. 2021);(Alquézar et al. 2022)). Alongside HLB, producers must cope with the intensification of abiotic stresses such as drought, salinity, and thermal extremes, as well as an increasing burden of viral and fungal pathogens ((Yesiloglu et al. 2022);(Dahro et al. 2023)). These pressures are exacerbated by the narrow genetic base of most cultivated varieties, which limits the availability of resilient alleles within the traditional gene pool. As a result, breeding efforts are increasingly turning toward exotic and underutilized germplasm to overcome these constraints and ensure long-term sustainability of citrus production ((Al-Khayri 2018);(Cimen et al. 2022)).

In this context, wide interspecific hybridization within the expanded *Citrus* genus offers a promising avenue for enhancing the adaptive potential of cultivated citrus. Crosses involving

phylogenetically distant species such as *C. australasica* (formerly *Microcitrus*), *C. glauca* (formerly *Eremocitrus*), or *C. trifoliata* (formerly *Poncirus*) now all taxonomically integrated within *Citrus* have yielded germplasm with unique traits, including drought tolerance, cold hardiness, and partial HLB tolerance ((Peng et al. 2020);(Alves et al. 2022);(Mahmoud et Dutt 2025)). Despite their potential, these lineages remain largely untapped in commercial breeding programs. Notably, *C. australasica* diverged from the main Asian citrus lineages during a distinct radiation event in the early Pliocene, approximately 4 million years ago (Wu et al. 2018), making it a particularly informative model to investigate the genomic consequences of wide hybridization, which integrates both authentic post-hybridization regulatory changes and the persistence of conserved intra-genus patterns.

Chromatin modifications, and especially DNA methylation, can impact gene expression *via* different pathways. In plants, DNA methylation occurs in three cytosine sequence contexts: CG, CHG, and CHH (where H = A, T, or C). CG methylation is maintained primarily by METHYLTRANSFERASE 1 (MET1), while CHG methylation depends on CHROMOMETHYLASE 3 (CMT3). CHH methylation is guided by both the RNA-directed DNA methylation (RdDM) pathway, involving DOMAINS REARRANGED METHYLTRANSFERASE 2 (DRM2), and the CMT2 pathway. These distinct but partially overlapping mechanisms ensure the establishment and maintenance of methylation across the genome, usually with a repressive role although it can vary depending on the context (Law et Jacobsen 2010). Together with other chromatin modifications such as histone post-translational modifications, DNA methylation patterns shape the epigenome. In the case of hybrids, it is not just two different genomes that are associated, but two different epigenomes, thus carrying both genetic and epigenetic variation.

Interspecific hybridization, is a common process in plants which enables the apparition of new phenotypes and species (Mason et Batley 2015). In breeding, this technique is widely used especially when hybrid vigor, also known as heterosis, is displayed in the F1 sibling. Heterosis is usually characterized in F1 by an increased biomass production and stress tolerance (Birchler et al. 2010). Recent sequencing approaches revealed that hybridization could be considered as a genomic and an epigenomic shock that, *in fine*, lead to the establishment of an hybrid specific transcriptional program which is not simply an addition of each parental transcriptional program (Hochholdinger et Yu 2025). In *Arabidopsis thaliana*, in rice, in maize and in cotton, DNA methylation and siRNA populations are altered in the hybrid. Changes to the hybrid methylome can occur in a way that differential methylation patterns inherited from the parent could be compensated to resemble each other, potentially *via* the action of small RNA (Greaves et al. 2015). However, this observation needs more evidence.

Creating hybrid resistant to pathogens, with a fruit pomology reaching the standard for citriculture is necessary to save a sector in great danger due to the various threats, in particular to diseases such the aforementioned HLB. The aim of the present study is therefore

not to identify resistance mechanisms per se, but to establish a haplotype-resolved framework to characterize allele-specific gene expression, DNA methylation, and small RNA accumulation in a complex interspecific citrus hybrid. To better understand these regulatory pathways, we analysed the expression profiles in a hybrid between two species separated by more than 4 million years of evolution, *Citrus reticulata* (mandarin) and *Citrus* (formerly *Microcitrus*) *australasica* (finger lime). In addition, to determine the impact of modifications to epigenetic signatures such as DNA methylation on this expression profile, we analysed the overall methylation of the genomes, but also of the associated small RNAs that enable them to be deposited in certain contexts. In the end, this study shows that these pathways participate in the establishment of differential allelic expression within the hybrid, but also that de novo methylation seems to play a particular role in citrus.

RESULTS

Assembly of an inter-specific citrus hybrid with a haplotype resolution

Although no direct genome comparison was performed prior to assembly, the two parental lines (*C. reticulata* and *C. australasica*) are known from phylogenetic studies to have diverged more than 4 million years ago (Wu et al. 2018). This long evolutionary separation suggests substantial sequence divergence between their genomes, likely including structural variation and high heterozygosity in their hybrid offspring. We therefore performed haplotype-resolved assembly rather than a conventional consensus assembly as previously published as trio-binning (Koren et al. 2018). We generated long-read sequencing using Oxford Nanopore Technologies of the hybrid individual with a 160X genome coverage using leaf tissue. To enable the assignment of hybrid long reads to their respective parental origins prior to assembly, we also obtained parental-specific k-mers from Illumina Tell-Seq libraries generated for each parent, as well short-read sequencing. This strategy allowed the realization of accurate trio-binning and independent reconstruction of both haplotypes (Figure 1A). Each assembled haplotypes consisted of only nine contigs, corresponding to the 9 chromosomes with a total assembly size of 349 Mb for *C. reticulata* and 359 Mb for *C. australasica*. The assemblies were highly contiguous (N50 = 38.0 Mb and 39.9 Mb, respectively; L50 = 4 for both) and exhibited consistent GC content (~34%).

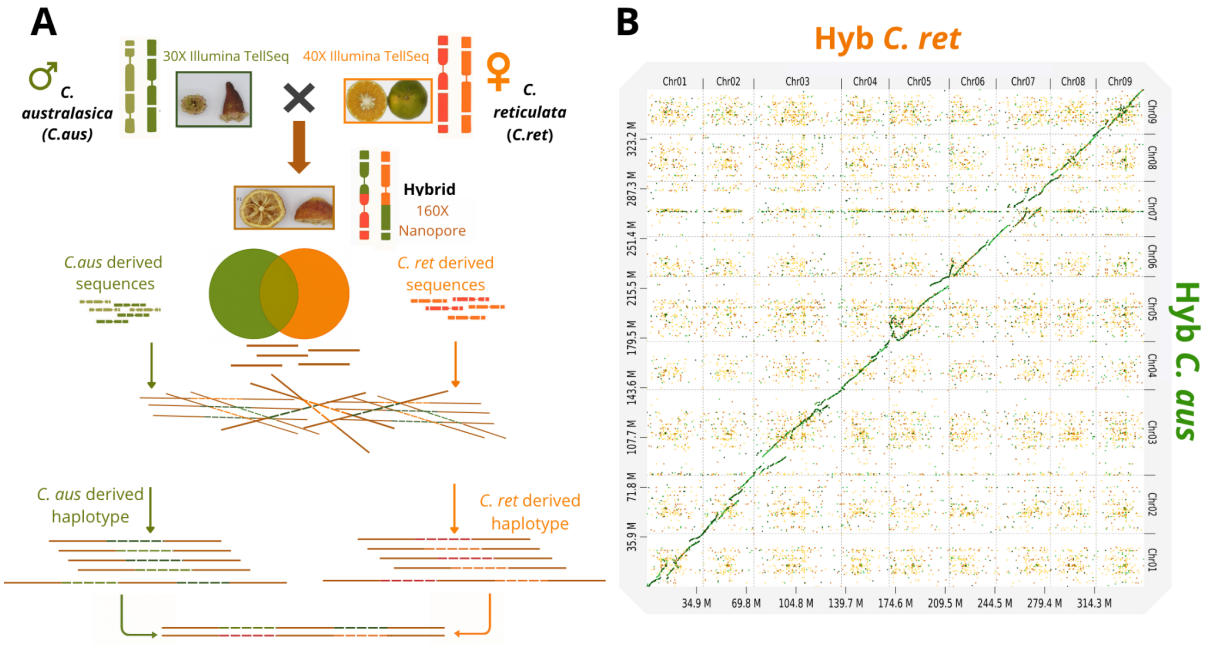

Figure 1. Haplotype-resolved genome assembly and structural variation.
*(**A**) Overview of the trio-binning genome assembly strategy used to generate haplotype-resolved assemblies of the citrus hybrid. Long reads from the hybrid were partitioned based on parental short-read data to generate separate assemblies corresponding to the maternal (C. reticulata, orange) and paternal (C. australasica, green) haplotypes. (**B**) Dot-plot alignment between the maternal (Hyb C. ret) and paternal (Hyb C. aus) genome assemblies showing overall synteny and structural rearrangements. Diagonal lines indicate homologous regions; off-diagonal signals reflect structural variations between haplotypes.*

To assess the assembly quality of both haplotypes, we anchored their pseudomolecules to a consensus *Citrus* genetic map (Ollitrault et al. 2024), constructed from seven *Citrus* species, including *C. australis* (an Oceanian species closely related to *C. australasica*) and *C. reticulata*. This anchoring was performed using the locOnRef tool from the Scaffhunter toolbox (Martin et al. 2016) allowing for the evaluation of synteny and collinearity between our assemblies and the reference map (Figure S1). The anchoring of each haplotype revealed a high degree of collinearity, with most chromosomes showing a clear one-to-one correspondence between physical and genetic coordinates. Minor discrepancies, visible as local discontinuities or small inversions in the Circos plots (Figure S1), likely reflect structural variants or orientation inconsistencies. These are expected when the available reference genomes differ from the actual parental genotypes used in the cross. Such local differences may also result from the trio-binning strategy, which preserves haplotypic divergence and can highlight micro-rearrangements between evolutionarily distant parental lineages. The absence of widespread inter-chromosomal misplacements and the consistent anchoring of large chromosome-scale scaffolds across linkage groups strongly support the structural accuracy of the haplotype-

185 resolved assemblies. These results confirm that the assembly strategy, despite the
186 unavailability of the actual parental genome sequences, produced high-quality haplotypes
187 with conserved chromosome architecture and minimal technical artifacts.
188 The two haplotypes' genomes are highly syntenic, although several structural variants can be
189 detected as shown by a dot plot analyses with the presence of numerous structural variations,
190 such as an inversion in the middle of the chromosome 1, a translocation on chromosome 3
191 and a large duplication on chromosome 5, for example (Figure 1B). Gene prediction *via BUSCO*
192 analysis revealed high completeness for both haplotypes (98.4% for *C. reticulata* and 98.3%
193 for *C. australasica*), with the majority of *BUSCO* present as unique or duplicated gene models
194 (see Table 1).
195
196

Statistic	***C. reticulata* Haplotype**	***C. australasica* Haplotype**
Genome size (Mb)	349	359
Number of contigs	9	9
N50 (Mb)	38.0	39.9
L50	4	4
%GC	34.13	34.10
BUSCO completeness (%)	98.4	98.3
Unique genes (%)	78.0	73.8
Duplicated genes (%)	19.7	24.5

197 ***Table 1*** *: Summary statistics for the contigs of the hybrid diploid genome assembled with an*
198 *haplotype resolution*
199
200 **Deciphering the differential allelic expression in the inter-generic hybrid**
201
202 Previous studies carried out on different combinations of hybrid plants have systematically
203 revealed the presence of differential allelic expression to a greater or lesser extent within the
204 hybrid compared with the parents, often for several hundred genes. To determine the
205 situation within the hybrid between *C. australasica* and *C. reticulata*, we carried out a
206 transcriptomic analysis in biological triplicate for the hybrid and each parent using leaf tissue.
207 Within the hybrid, the transcripts were mapped onto the haplotype genomes in order to
208 obtain an allelic resolution of the expression level of each of the genes.
209
210 To analyse differential gene expression between the two sub-genomes, we identified a
211 common gene pool. Gene models were transferred from the reference *CITRE* (Droc et al.

212 2024) to each haplotype assembly using Liftoff (Shumate et Salzberg 2021). Liftoff is a stand-
213 alone lift-over tool that takes as input the reference genome sequence (FASTA), the target
214 genome sequence (FASTA), and the reference gene annotation (GFF/GTF) even if assembled
215 genomes accumulate structural variation and divergence. It uses Minimap2 (H. Li 2018) to
216 map each reference gene's sequence onto the target assembly, and for each gene selects the
217 set of exon alignments that maximizes sequence identity while preserving the exon–intron
218 structure. Using this strategy, 95.0% of the (*CITRE*, ((Droc et al. 2024)) reference genes (33,055
219 out of 34,798) were successfully transferred to the maternal haplotype, and 89.0% (30,980
220 out of 34,798) were annotated on the paternal haplotype. Among these, 30,980 orthologous
221 genes were found in both haplotypes and represent our pool of common genes.
222
223 We were thus able to determine which genes showed differential bias in transcript
224 accumulation, and counted 1758 genes in which the contribution of the allele derived from
225 *C. australasica* was at least 3 times greater, and 1809 genes in which the contribution of the
226 allele derived from *C. reticulata* was 3 times greater within the hybrid (Figure 2A). Some
227 transcript accumulation profiles were confirmed using RT-qPCR (Figure S2 and Table S3).
228
229

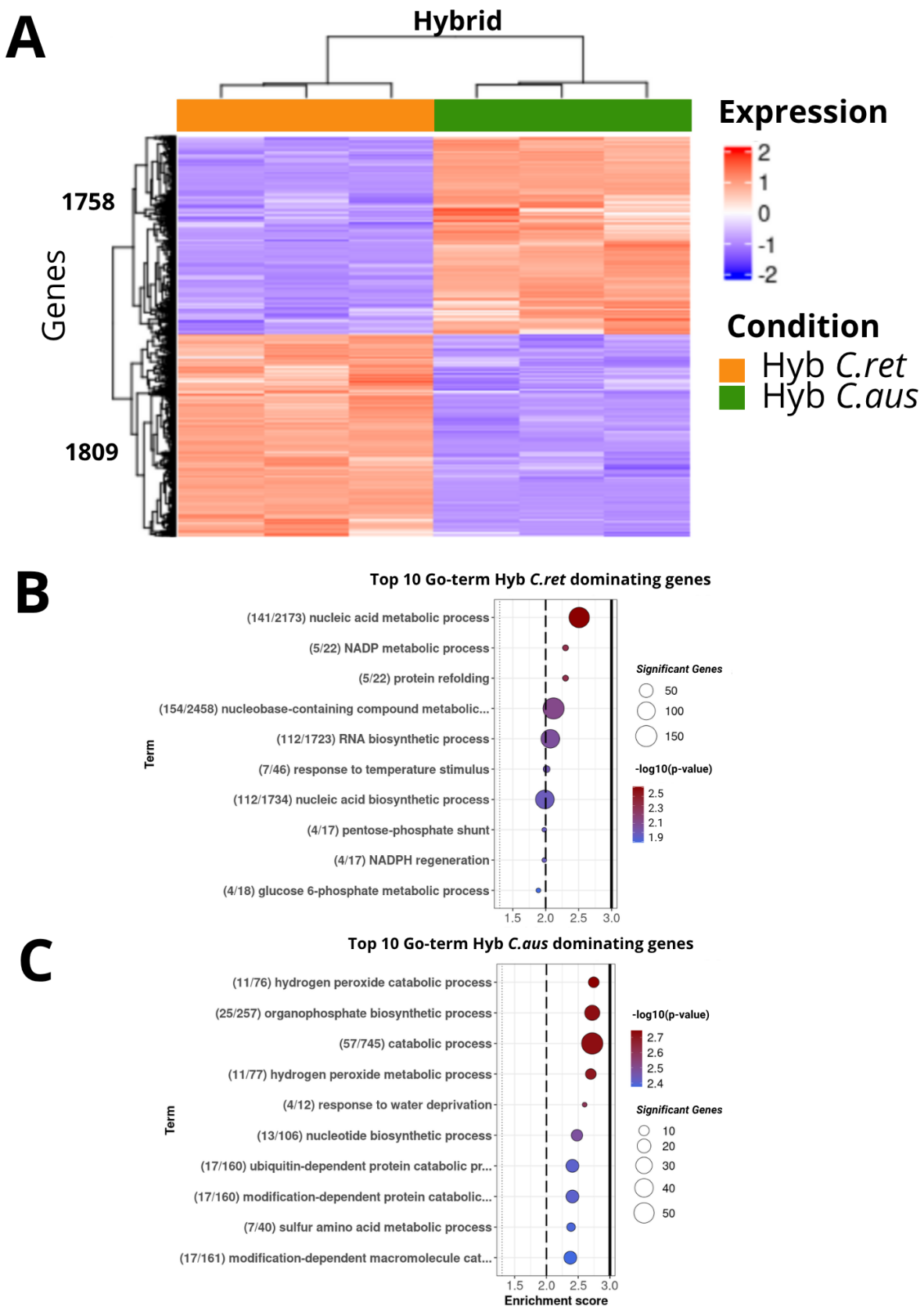

Figure 2. Allele-specific expression and functional enrichment in the hybrid.

*(**A**) Heatmap showing allele-specific expression between the two haplotypes in the hybrid. Expression values are variance-stabilized counts (VST) obtained from DESeq2 and centered*

*gene-wise (z-score). Rows represent genes; columns represent biological replicates of the two hybrid haplotypes. The colour gradient reflects standardized expression levels: red indicates higher expression, blue indicates lower expression (unit: log_2-transformed normalized expression). (**B**) Bubble plot of enriched GO Biological Process terms among genes upregulated on the maternal haplotype. Bubble size represents gene count; colour reflects enrichment p-value. (**C**) Bubble plot of enriched GO terms among genes upregulated on the paternal haplotype, plotted as in panel (**B**).*

We then determined whether certain classes of genes were particularly affected by this differential expression by determining changes in transcript accumulation according to gene ontology (GO term). Several groups of genes were found to be significantly differentially expressed within the hybrid. The *C. reticulata* haplotype is dominant for genes involved in metabolic processes for nucleic acid and NADP, while the *C. australasica* haplotype is dominant for genes implicated in catabolic processes particularly hydrogen peroxide, as well as in organophosphate biosynthetic processes (Figure 2B and 2C and Figure S3).

Such dominance at the GO term scale implies a biased implication of one of the parents in the hybrid in the regulation of certain metabolic and physiological pathways that could explain partially the phenotype observed in the hybrid.

Finally, we identified 289 and 268 genes in the hybrid that are exclusively expressed either by the *C. australasica* or the *C. reticulata* haplotypes respectively (Figure S4). Again, these numbers are very similar, demonstrating a somewhat overall balance between the two haplotypes. In both cases, the majority of these genes are only expressed in the corresponding parental lines (Figure S4).

DNA methylation landscape in hybrid haplotypes reveals context- and parent-specific reprogramming

To determine whether some of this differential allelic expression may be the result of changes operating at the epigenetic level, we analysed cytosine methylation globally for the hybrid and each parent using leaf tissue. Whole-genome Bisulfite sequencing (WGBS) approaches were used and sequenced using 150bp paired-reads with depth of coverage equivalent to 20 times the average citrus genome size in biological triplicate.

Overall levels of DNA methylation revealed distinct patterns across the three cytosine contexts (Figure 3A). Methylated CG (mCG) were the most abundant, followed by methylated CHG and methylated CHH (mCHG and mCHH). Both hybrid haplotypes displayed a significant reduction in CG methylation relative to their respective parents, with Hyb *C. ret* showing a 5.2% decrease and Hyb *C. aus* a 5% decrease compared to *C. reticulata* and *C. australasica*, respectively. In contrast, mCHG levels were relatively stable across hybrids and parents.

Notably, mCHH showed a haplotype-specific reprogramming: while Hyb *C. ret* maintained mCHH levels comparable to *C. reticulata*, Hyb *C. aus* exhibited a clear increase compared to *C. australasica*, suggesting targeted activation of RdDM in the paternal haplotype.

At the chromosomal scale, genome-wide methylation distribution showed mCG and mCHG highest in pericentromeric regions, correlating with repetitive element abundance (Figure S5) (Giraud et al. 2025). Methylated CHH was generally lower but showed local peaks more pronounced in Hyb *C. aus* than Hyb *C. ret*, supporting reinforced RdDM activity targeting the *C. australasica* haplotype.

We then validated the methylation pattern observed using WGBS in the hybrid by analysing five different promoter regions that either accumulate or do not accumulate cytosine methylation using BS-PCR followed by Sanger sequencing (Figure S6 and table S3). Next, we analysed DNA methylation patterns across gene bodies and their flanking regions using metaplot analyses. In CHG and CHH contexts, methylation dropped sharply within gene bodies, with elevated levels in flanking regions (Figure 3B). mCHH around genes was markedly higher in *C. australasica* haplotype than in *C. reticulata* haplotype, reinforcing the idea of RdDM-driven reprogramming is more pronounced on the *C. australasica*-derived haplotype. Levels of mCG between the hybrid haplotypes were minor at the genic level, but a modest decrease in the *C. reticulata* haplotype was noted in promoter-proximal regions, whereas gene-body mCG remained relatively stable and high in both hybrids. These patterns reflect the complex locus- and context-specific DNA methylation reprogramming reported during cellular differentiation and hybridization ((Kakoulidou et Johannes 2024);(Lauss et al. 2018)) Direct comparisons between each hybrid haplotype and its respective parent confirmed an asymmetric pattern of methylation reprogramming (Figure 3B). Hyb *C. aus* showed increased mCHH compared to *C. australasica*, particularly in gene-flanking regions, while mCG was largely conserved. Hyb *C. ret* exhibited slightly elevated mCG relative to *C. reticulata*, with stable mCHH levels. This supports models where epigenetic remodelling in hybrids is haplotype-specific and influenced by parental origin, consistent with findings that DNA methylation remodelling in hybrids is often driven by epigenetic interactions and small RNA pathways (Kakoulidou et al. 2024).

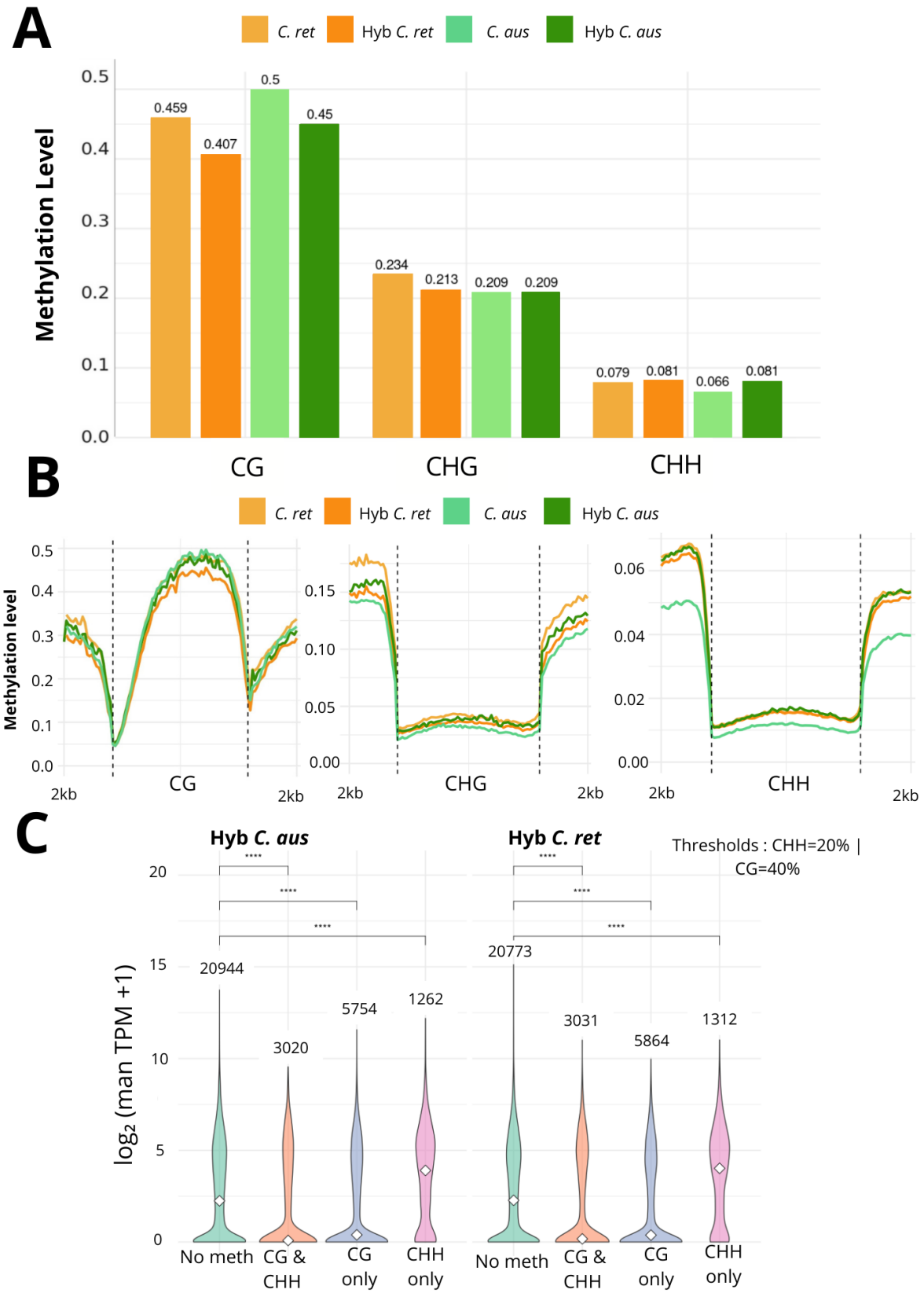

Figure 3. DNA methylation profiles and correlation with gene expression.

(A) *Global DNA methylation levels (in %) in CG, CHG, and CHH contexts across parental haplotypes (C. reticulata, C. australasica) and their corresponding haplotypes within the hybrid. Values indicate mean methylation levels across all annotated genes.* ***(B)*** *DNA*

methylation metaprofiles (in %) across gene bodies and ±2 kb flanking regions in each cytosine context. Curves represent average methylation profiles for each genotype and context. ***(C)*** *Violin plots showing gene expression levels (log_2(mean TPM + 1)) according to promoter methylation status in CG and CHH contexts in the two haplotypes of the hybrid. Promoters are categorized into four classes: "No methylation", "CG & CHH", "CG only", and "CHH only" based on thresholds (CHH ≥ 20%, CG ≥ 40%). Statistical differences in expression across categories were assessed using a Kruskal–Wallis test ($p < 0.05$), followed by pairwise Dunn's post-hoc comparisons with Benjamini–Hochberg correction. The number of genes in each category is indicated above each violin. Asterisks denote significance levels from post-hoc comparisons: * = padj < 0.05, ** = padj < 0.01, *** = padj < 0.001, **** = padj < 1e-4.*

We then looked at the impact of this methylation, whatever its context, on gene expression within the hybrid, with the idea of evaluating this type of epigenetic modification on the establishment of the differential allelic expression previously observed. For each haplotype, we analysed the relative expression of the genes when their promoter region (1 kb upstream of the transcription start site, TSS) was either unmethylated, or methylated at CG (at least 40%), or methylated at CHH (at least 20%), or both. As expected, genes whose promoters accumulate only mCG or both mCG and mCHH are strongly correlated with a low level of expression (Figure 3C), whatever the haplotype, compared to non-methylated promoters. In contrast, promoter regions only accumulating mCHH associate significantly with genes with a higher expression level than those without mCG only, both mCG and mCHH or in comparison with those that are unmethylated (Figure 3C). We also confirmed this result by analysing numerous genes where indeed high gene expression was not incompatible with the presence of small clusters and mCHH accumulation in their promoter (Figure S7). Taken together, our data reveal the presence of significant changes at the methylation levels, with contrast impact on gene expression depending on the cytosine context.

Small RNA population and impact in the intergenic hybrid

In plants, mCHH accumulation in promoter regions is the result of the action of RdDM and RNA polymerases IV and V, which are specific to plants and enable the generation of small 24 nt RNA (hereafter named siRNA). Associated with an Argonaute protein (AGO4 in *A. thaliana*), these siRNA are then able to target sites for CHH methylation *via* the action of DRM2 (Matzke et al. 2015). Therefore, we expect that at least some of the promoters accumulating CHH methylation will also accumulate siRNA. To test this hypothesis, we performed small RNA-seq analyses for the hybrid and each parent using leaf tissue in triplicates.

Small RNA were grouped according to their size, showing the presence of two major types of small RNA: those of 21-nt, corresponding to microRNA, and those of 24-nt, which are more abundant and correspond to siRNA (Figure 4A) (Zhan et Meyers 2023). Overall, we can see

353 that the two haplotypes participate equally in the production of these smallRNAs in
354 quantitative terms (Figure 4B).
355
356 We then focused on the siRNA, responsible for targeting genomic regions in CHH methylation
357 *via* the RdDM pathway. To analyse whether these siRNA target the same regions, we mapped
358 them on the haplotype-resolved hybrid genomes. A third of the individual siRNA originates
359 from both subgenomes, while the other two-thirds originate either from *C. reticulata* or *C.*
360 *australasica*-derived haplotype (Figure S8). Because of the important sequence variation
361 existing between the two haplotypes, we decided to question their functional impact once
362 grouped into clusters when their coverage peaks were located within a 200-nucleotide
363 window, as defined by ShortStack. Promoters targeted solely by CHH methylation are
364 expected to be targeted by siRNA which then participate in the recruitment of DRM2 at
365 promoter regions, then genes whose promoters are targeted by siRNA should also be more
366 transcribed overall.
367
368 We therefore focused on the siRNA clusters targeting only the promoter regions (1 kb
369 upstream of the TSS). Once again, the majority of siRNA groups were produced by only one
370 of the two haplotypes within the hybrid. Only 25% were produced simultaneously by both
371 haplotypes in the hybrid (Figure 4B). Among these haplotype-specific siRNA clusters, only half
372 are also expressed in the parental lines (Figure 4C), highlighting a potential asymmetric
373 inheritance. Finally, we analysed the global expression of the genes targeted or not by siRNA
374 clusters in their promoter and demonstrated that those with targeted promoters accumulate
375 more transcribed than those non-targeted in their promoter (Figure 4D). Altogether, these
376 results demonstrate not only that the contribution of siRNA is essentially haplotype-
377 dependent within the hybrid, but also that the targets of siRNA tend to be more transcribed,
378 supporting the hypothesis of a potential involvement of RdDM in transcriptional activation
379 within the hybrid.
380
381
382

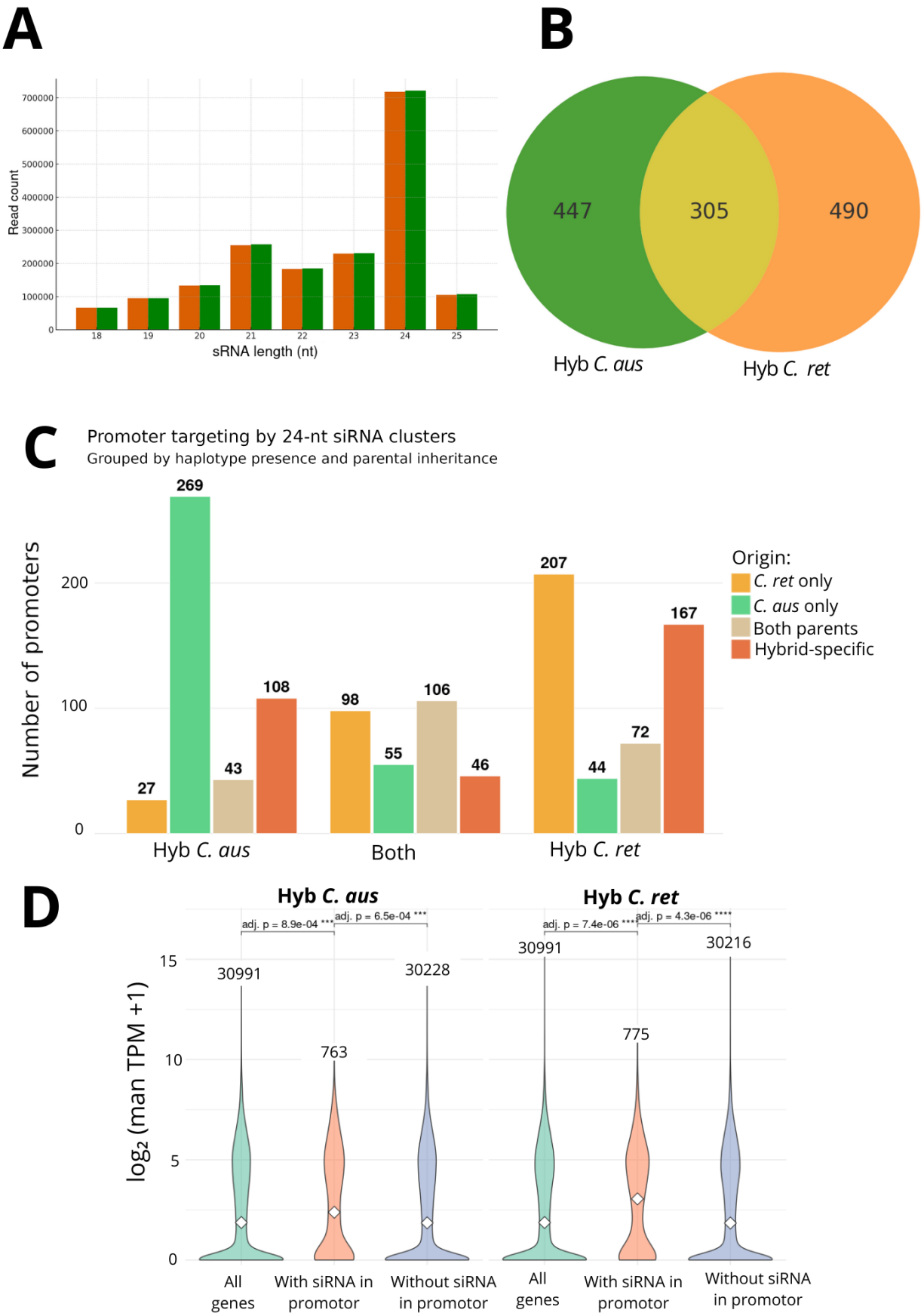

Figure 4. Haplotype-specific distribution and effects of 24-nt siRNA clusters.

385 ***(A)*** *Size distribution of mapped small RNAs in each hybrid haplotype.* ***(B)*** *Venn diagram*
386 *showing the overlap of 24-nt siRNA clusters between the two haplotypes of the hybrid. The*
387 *intersection represents clusters targeting the same promoters in both haplotypes.* ***(C)***
388 *Classification of gene promoters targeted by 24-nt siRNA clusters in the hybrid, based on*
389 *parental origin. Promoters are grouped according to whether they are targeted by siRNA*
390 *clusters inherited from C. reticulata only (orange), C. australasica only (green), both parents*
391 *(beige), or are hybrid-specific (red).* ***(D)*** *Violin plots showing gene expression levels*
392 *(log_2(TPM+1)) depending on the presence or absence of 24-nt siRNA clusters in promoters, for*
393 *each hybrid haplotype. Genes with siRNA in their promoters tend to be more expressed than*
394 *those without (Wilcoxon test, adjusted p-values indicated).*
395
396 **Impact of RdDM on differentially expressed genes (DEG) in the hybrid**
397
398 To explore the impact of hybridization on the interrelation between gene expression, DNA
399 methylation, and siRNA production, we integrated our epigenomic data at the haplotype level
400 (Figure 5A–B). We then performed several statistical analyses of gene expression within the
401 hybrid, quantified as TPM.

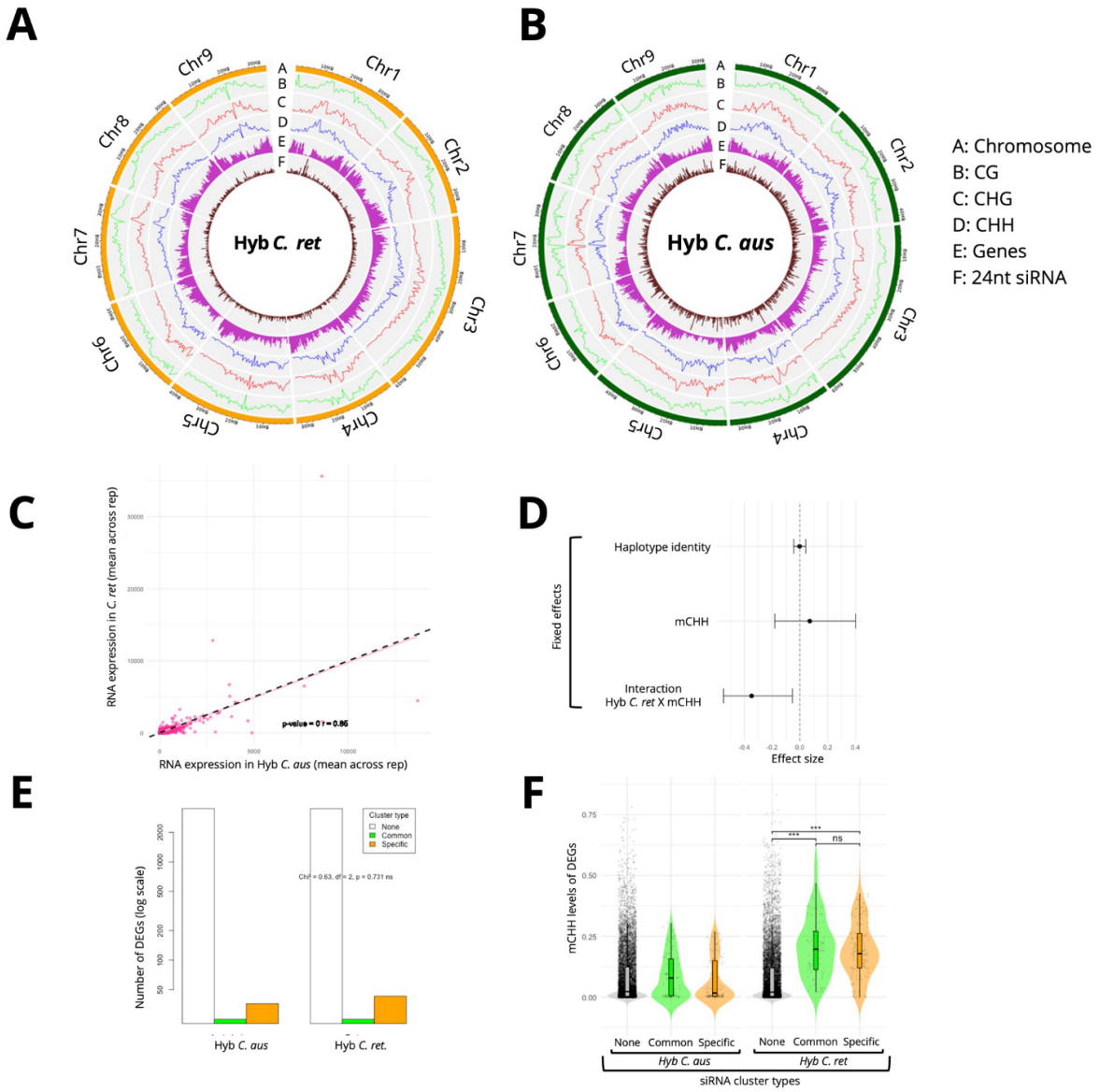

Figure 5. Genome-wide epigenomic patterns and overlap with expression.

*(**A–B**) Circos plots representing genome-wide profiles of DNA methylation, gene density, and 24-nt siRNA clusters across the nine chromosomes of the two haplotypes of the hybrid: (**A**) C. reticulata-derived haplotype (orange) (**B**) C. australasica-derived haplotype (green). Tracks from outer to inner rings: A : Chromosomes; B–D : DNA methylation levels in CG (red), CHG (blue), and CHH (purple) contexts; E : Gene density; F : Density of 24-nt siRNA clusters. (**C**) Spearman's rank correlation in gene expression between haplotypes. (**D**) Effect sizes (±95% CI) from a linear mixed model evaluating the impact of haplotype, mCHH levels, and their interaction on DEG expression (TPM). Contrasts are treatment-coded with C. australasica haplotype as the reference. CIs overlapping zero indicate non-significance. (**E**) DEG distribution by siRNA cluster types and haplotypes (None = no cluster, Common = shared, Specific = haplotype-specific). (**F**) mCHH levels across small RNA cluster types by haplotype. Dunn's test with Bonferroni correction: Significance: *** $p \leq 0.001$, ** $p \leq 0.01$, * $p \leq 0.05$, ns = not significant.*

First, we tested whether gene expression levels were correlated between haplotypes using Spearman's rank correlation in R. We observed a strong and highly significant correlation (Spearman's $\rho = 0.85$, $p < 2.2 \times 10^{-16}$), closely following a 1:1 relationship (Figure 5C), suggesting that most genes exhibit similar expression levels across the two haplotypes. We then tested whether the 3,567 DEG within the hybrid were influenced by haplotype identity, mCHH levels, or the interaction between the two. We used a linear mixed-effects model with haplotype identity, mCHH and the interaction included as fixed effects, while the first principal component (PC1) from a PCA of gene expression profiles was included as a random effect. This approach captures underlying clustering or co-expression patterns between genes that could confound the interpretation of haplotype and methylation effects. The model revealed no overall differences in gene expression of DEG between haplotypes, confirming that neither haplotype systematically dominates the other in terms of expression of DEG (Top; Figure 5D). It also showed that mCHH alone had no consistent effect on gene expression on DEG (Middle; Figure 5D). However, a significant interaction between haplotype identity and mCHH levels was detected (Bottom; Figure 5D): a marked reduction in gene expression was specifically observed when mCHH occurred on the *C. reticulata* haplotype compared to *C. australasica* haplotype. This suggests that the effect of mCHH on gene expression of DEG is haplotype-dependent.

We then investigated the impact of hybridization on siRNA clusters on promoters of DEG. We categorised clusters in three classes: "Specific" (detected in only one haplotype), "Common" (shared between both), and "None" (genes with no detected cluster in their promoter). We counted the number of DEG per category and haplotype, and used a Pearson's Chi-squared test of independence to assess differences in distribution. The distribution of siRNA cluster types did not significantly differ between haplotypes ($Chi^2 = 0.63$, df = 2, $p = 0.73$). Most DEG lacked a detectable cluster in both haplotypes, and the proportions of "Common" and "Specific" clusters were similar across haplotypes (Figure 5E). These results suggest that the presence or specificity of siRNA clusters among differentially expressed genes is similar across haplotypes.

Finally, to test whether mCHH levels differed on promoter regions targeted by siRNA clusters according to their origin, we performed another test, still focusing on DEG. Since methylation data did not follow a normal distribution, we used non-parametric Kruskal-Wallis rank sum tests to compare methylation levels across cluster types ("None", "Specific", "Common") separately for each haplotype. In the *C. australasica* haplotype, mCHH levels did not differ significantly between cluster types ($\chi^2(2) = 2.35$, $p = 0.31$). No pairwise comparisons were significant after correction. In contrast, *C. reticulata* haplotype showed a significant effect of siRNA cluster type on mCHH ($\chi^2(2) = 232.25$, $p < 2.2\times10^{-16}$). Post hoc tests revealed that DEG with no associated siRNA cluster had significantly lower methylation than those with either "common" or "specific" clusters ($p < 0.001$ for both comparisons). Moreover, there was no significant difference between "common" and "specific" clusters ($p = 0.67$ after Bonferroni

458 correction). These results suggest that in *C. reticulata* haplotype, the presence of a siRNA
459 cluster regardless of whether it is shared or specific is associated with an increase in mCHH,
460 whereas in *C. australasica* haplotype, mCHH is not significantly affected by cluster occurrence
461 (Figure 5F).
462
463 **Association of RdDM with expressed genes is not linked to hybridization**
464
465 Our strategy revealed that while for the majority of genes, the parental contribution to
466 transcript accumulation within the hybrid was balanced, around 10% of common genes were
467 dominated by the contribution of just one of the two parents. This dominance is even more
468 marked for siRNA, where only a third are expressed by both haplotypes.
469
470 Genome-wide analyses showed that cytosine methylation, across CG, CHG, and CHH contexts,
471 accumulates in gene-poor regions near the chromosomal centres, likely corresponding to
472 centromeric or pericentromeric regions, despite centromeres not being clearly annotated in
473 Citrus (Xia et al. 2020). Both haplotypes display consistent patterns of mCHH and siRNA
474 accumulation in these regions, indicative of canonical RdDM activity, potentially targeting
475 transposable elements. The strong co-localization of mCHH and siRNA in pericentromeric
476 regions further supports their coordinated role in heterochromatin maintenance, although
477 siRNA-independent mCHH accumulation may also be involved ((Stroud et al. 2014) ; (He et al.
478 2021)). Despite the interspecies nature of the hybrid (*C. reticulata* × *C. australasica*), the
479 epigenomic landscapes of both haplotypes show remarkable global symmetry. This conserved
480 chromosomal organization suggests that genome compartmentalization and RdDM activity
481 are stable features across divergent Citrus lineages and may contribute to the overall
482 transcriptional stability observed in the hybrid (Figure 5A–B), although a potential, we
483 identified a haplotype-bias impact in the hybrid for DEG (Figure 5F).
484
485 To assess whether RdDM is linked to transcriptional activity, we analysed gene expression
486 levels in relation to both mCHH accumulation and siRNA presence. As previously shown,
487 analysis of expression data with either cytosine methylation or the presence of siRNA
488 revealed that genes were more highly expressed when they either accumulated mCHH (Figure
489 3) or were targeted by siRNA (Figure 4). To see if these two aspects are linked, we analysed
490 all the genes targeted by siRNA and that also accumulate at least 20% mCHH in their promoter
491 region, separating the expressed genes (Figure 6A) from the genes that are little or no
492 expressed (Figure 6B). Remarkably, genes whose promoters accumulate these two
493 characteristics are 10 times more likely to be associated with expressed than unexpressed
494 genes. However, these targeted genes are only targeted within the hybrid in at least half the
495 cases: in 49% of cases (93 promoters out of 191) when the genes are associated with
496 expression (Figure 6A) and in 77% of cases (24 promoters out of 31) when the genes are not
497 or only slightly expressed (Figure 6B).
498

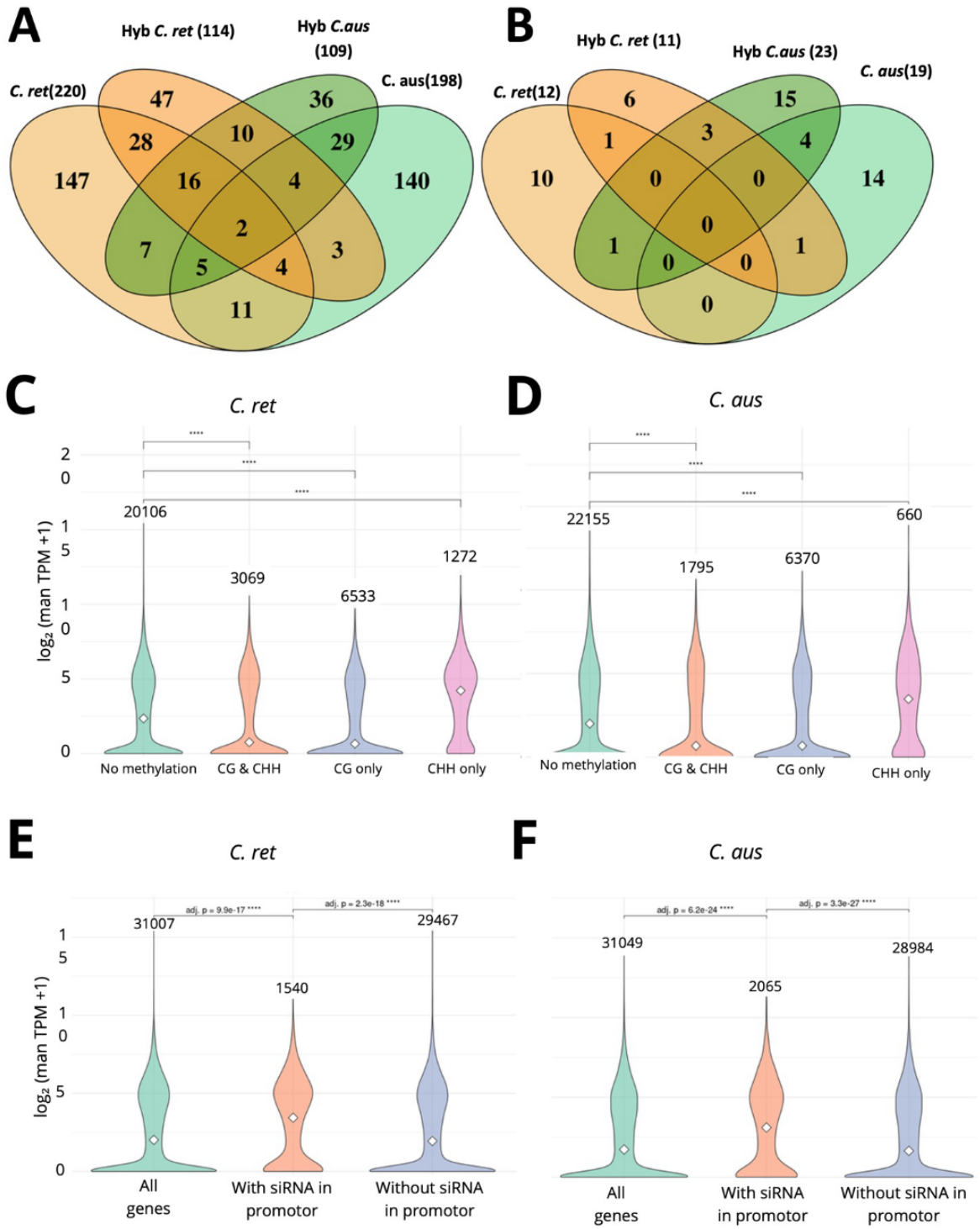

Figure 6. Epigenetic regulation of gene expression in the parental genomes.

*(**A–B**) Venn diagrams showing the overlap of genes whose promoters are targeted by 24-nt siRNA clusters across parental and hybrid haplotypes. (**A**) Expressed genes (TPM > 1) with promoter siRNA clusters. (**B**) Non-expressed genes (TPM ≤ 1) with promoter siRNA clusters.*

Each subset indicates the number of genes whose promoters are targeted by siRNA in one or more haplotypes. ***(C–D)*** *Violin plots showing gene expression levels (log_2(mean TPM + 1)) in parental genomes:* ***(C)*** *C. reticulata,* ***(D)*** *C. australasica. Genes are grouped according to promoter methylation status: No methylation, CG only, CHH only, and CG & CHH, using thresholds of 40 % CG and 20 % CHH methylation. Numbers above each plot indicate the number of genes in each category. Asterisks indicate significant differences (Wilcoxon test, **** = p < 1e-4).* ***(E–F)*** *Gene expression comparison based on the presence or absence of 24 nt siRNA clusters in promoters for:* ***(E)*** *C. reticulata,* ***(F)*** *C. australasica. Wilcoxon rank-sum tests were used to assess statistical differences; adjusted p-values are indicated (Benjamini–Hochberg correction).*

To test whether RdDM targets are also associating with higher expression in the parental lines, we analysed the transcriptomic, DNA methylation and small RNA data in the parents, using the haplotype resolved reference genome of the hybrid (Figure S9). Interestingly, mCHH is also linked to high gene expression in the parental lines, which goes to show that this atypical correlation is not linked to hybridization *per se*, but would rather be a more general feature in *Citrus* genus. A closer examination of siRNA–CHH methylation modules shows that both CHH methylation and siRNA accumulate specifically within the 1 kb region upstream of the transcription start site (TSS), mostly at expressed genes (Figure S10).

To confirm this hypothesis, we perform the same analyses made on the hybrid haplotype individually on methylation and siRNA accumulation in the parental lines, and indeed confirm a similar association of expressed genes with siRNA cluster or with only mCHH both in *C. reticulata* (Figure 6C and E) and in *C. australasica* (Figure 6D and F). *In fine*, in both *C. reticulata* and *C. australasica*, genes with promoter accumulating mCHH and/or siRNA clusters were more likely to be expressed than genes without these marks, reinforcing the conclusion that this epigenetic pattern is conserved across species. Venn diagram analysis further showed partial overlap between mCHH and siRNA-targeted genes in each parent (Figure S11), suggesting that these two layers of RdDM regulation may act independently or additively.

To assess whether this profile is shared across citrus species, we took advantage of the published RNA-seq and WGBS-seq data in citrus lemon (*Yu H. et al., 2024).* Again, a significant higher expression is also observed for the 783 genes that accumulate CHH methylation in their promoter (Figure 7, left panel). Moreover, as only leaf tissue has been analysed so far, we also analysed the correlation between gene expression and accumulation of CHH methylation only in the promoter for other citrus and related species, this time using root tissues (Figure 7). WGBS and RNA-seq analyses, from *C. reshni* (Cleopatra mandarin, a member of *C. reticulata*) and *Poncirus trifoliata,* were performed for this study. In addition, we also re-analysed advantage of the methylation and expression data previously published for *C. sinensis* (Huang et al., 2021). In these three species, we were able to confirm a significant increase in gene

545 expression when CHH-only methylation accumulates in gene promoters (1 kb upstream of the
546 TSS) (Figure 7).
547 Altogether, these results support a model in which RdDM-associated targeted genes are
548 positively associated with gene expression in *Citrus*, and this association is conserved across
549 divergent species. If the results suggest stable associations across datasets, they do not
550 strictly exclude the influence of stage- or environment-specific factors.
551

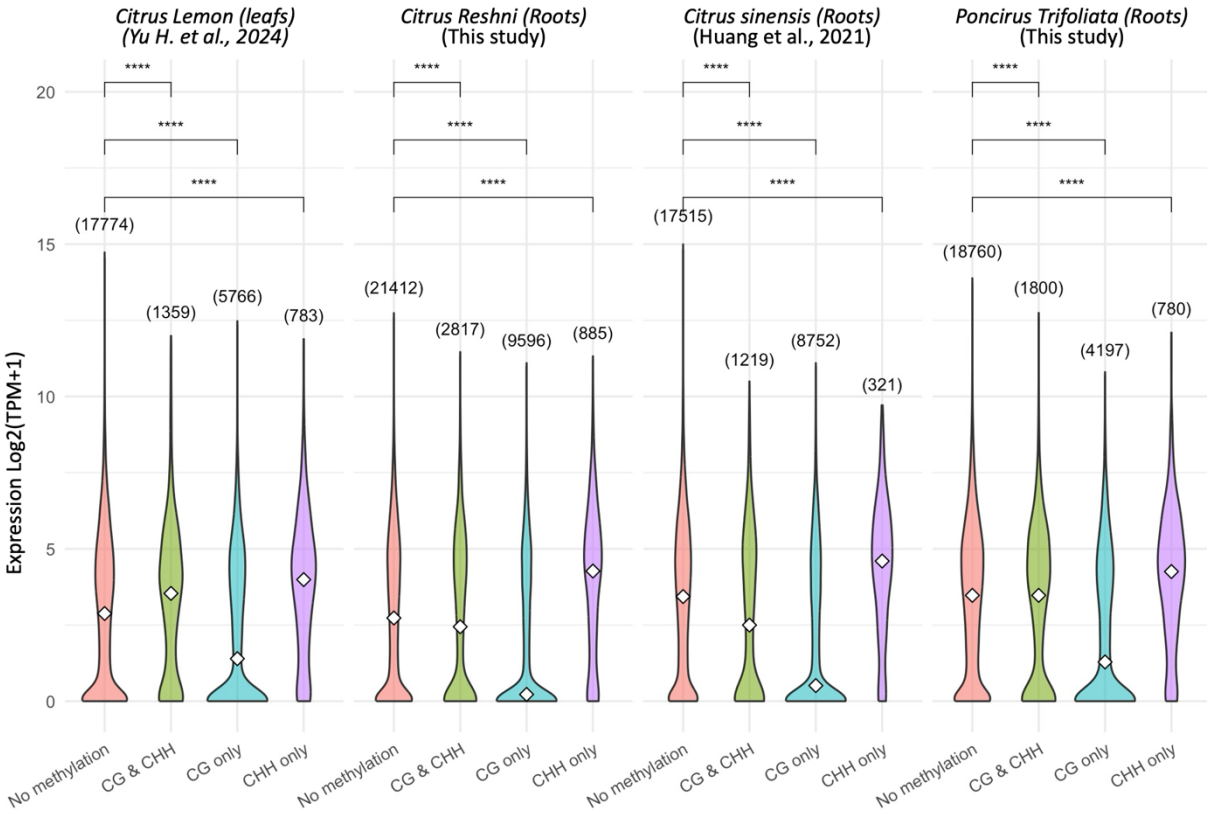

552
553 ***Figure 7: Correlation between DNA methylation and expression profiles in root and shoot***
554 ***tissues for Citrus and related species.***
555 *Violin plots showing gene expression levels (log_2(mean TPM + 1)) according to promoter*
556 *methylation status in CG and CHH contexts in Citrus lemon, Citrus Reshni, Citrus sinensis and*
557 *Poncirus trifoliata. Promoters are categorized into four classes: "No methylation", "CG &*
558 *CHH", "CG only", and "CHH only" based on thresholds (CHH ≥ 20%, CG ≥ 40%). Statistical*
559 *differences in expression across categories were assessed using a Kruskal–Wallis test ($p <$*
560 *0.05), followed by pairwise Dunn's post-hoc comparisons with Benjamini–Hochberg*
561 *correction. The number of genes in each category is indicated above each violin. Asterisks*
562 *denote significance levels from post-hoc comparisons: **** = padj < 1e-4.*
563
564 **DISCUSSION**
565
566 In this study, we investigated the transcriptional and epigenetic consequences of an
567 interspecific hybridization event between two phylogenetically distant *Citrus* species
568 separated by over 4 million years of divergence: *C. reticulata* and *C. australasica*. By

569 integrating high-quality haplotype-resolved genome assemblies with transcriptome, DNA
570 methylation, and small RNA datasets, we provide new insights into the regulatory dynamics
571 occurring in such distant hybrid. To analyse the citrus hybrid and its parent, we developed a
572 pipeline adapted to the integration of genomic and epigenomic data with a haplotype
573 resolution using the strategy previously published in (Koren et al. 2018) and that resolves
574 allelic variation before assembly. This trio-binning approach enabled the separation of two
575 highly divergent haplotypes and produced chromosome-scale assemblies with high contiguity
576 and collinearity (Figure1 and S1). The observed structural variants, including small inversions
577 and local discontinuities, may reflect true polymorphisms between the actual parental
578 genomes or arise from hybrid-specific chromosomal rearrangements. While the assemblies
579 already provide a robust foundation for genomic comparisons, future polishing steps, for
580 example through the integration of Hi-C data, could further improve scaffold orientation and
581 help distinguish between biological rearrangements and minor assembly inconsistencies.
582 More importantly, the haplotype-resolved assembly provided the basis for identifying
583 differentially expressed genes with allelic resolution in the hybrid. Because all analyses were
584 conducted under non-stressed conditions, in the absence of both biotic and abiotic
585 challenges, the regulatory patterns described here should be interpreted as a basal,
586 haplotype-resolved framework rather than as direct evidence of stress- or disease-resistance
587 mechanisms.
588
589 Hundreds of expressed genes accumulate transcripts mainly from only one of the parental-
590 derived genomes, which implicate a certain dominance at the gene scale (Figure 2, S3 and S4).
591 Although some metabolic or catabolic pathways are enriched among the dominant genes, we
592 do not know at this stage the impact of this imbalanced expression. However, we can note
593 that this imbalance seems to be somehow equilibrated between the two parent-derived
594 genomes since a similar number of DEG are found in the haplotype-resolved hybrid
595 transcriptome.
596
597 At the methylation level, the global epigenomic landscapes were remarkably conserved
598 between haplotypes, closer inspection of Figure 5A–B reveals subtle but potentially
599 meaningful differences in local siRNA accumulation. Discrete siRNA peaks specific to one
600 haplotype, particularly on chromosomes 6 and 9, may reflect species-specific bursts of
601 transposable element (TE) activity or structural rearrangements. These features could mark
602 regions of differential genome organization between *C. reticulata* and *C. australasica,* but
603 definitive interpretation will require high-quality TE annotation of each phased haplotype.
604
605 Quantitatively, if a global decrease in mCG and mCHG is observed in the hybrid compared to
606 the parent, mCHH is slightly higher, suggesting a particular role or deregulation of the RdDM
607 pathway. Interestingly, mCHH only significantly affects DEG derived from the *C. reticulata*
608 haplotype (Figure 5D and S12). This haplotype-specific mCHH methylation is accompanied by
609 a specific accumulation of siRNA in the *C. reticulata* haplotype promoter of DEG (Figure 5F).

610 The reason why only one haplotype seems to be sensitive to RdDM is not clear. mCHH
611 accumulation in the hybrid seems to be additive, reaching the highest level of the parent as
612 shown in (Figure 3B). In consequence, we detected an increase in the level of mCHH of around
613 50% throughout the genome of the *C. australasica* haplotype compared to the parental line.
614 This increase, in one generation, is considerable and could probably explain at least partially
615 why mCHH do not have as much impact on gene transcriptional regulation in the *C.*
616 *australasica* haplotype than in the *C. reticulata* haplotype, within the hybrid. One explanation
617 could be that because of the sequence variation between the two haplotypes, mCHH readers
618 may act preferentially on their own haplotype genome and a 50% increase is probably due to
619 deregulation and/or an imbalance that cannot be corrected in this generation, saturating
620 mCHH reader belonging to the *C. reticulata* haplotype. In addition, we cannot entirely rule
621 out the potential impact of stage- or environment-specific factors. Previous studies in *A.*
622 *thaliana* hybrids demonstrated that altered DNA methylation and siRNA patterns exist in the
623 hybrid, potentially contributing to the hybrid vigor phenotype (Greaves et al. 2015). However,
624 in that case, an increased mCG and a decreased mCHH has been observed relative to the
625 parents (Greaves et al. 2012), which is the reverse of our observation here. Further
626 transcriptional and epigenetic analyses on future generations will show whether this
627 imbalance persists.
628
629 We suggest that the RdDM pathway is much more implicated in transcriptional activation,
630 than repression in *Citrus*. One hypothesis could be that the RdDM pathway is affected in
631 citrus, with transcriptional regulation affecting DNA methylation deposition or maintenance.
632 However, the expression profile of the major members of the pathway appears stable in the
633 hybrid and parents (Figure S13). As a fact, we identified hundreds of highly expressed genes
634 in the hybrid, but also in the parental lines that accumulate both mCHH to a level higher than
635 20%, and that are also targeted by siRNA at their promoter. This number of targets is probably
636 higher since it cannot be ruled out that the lack of detection of siRNA clusters is not the result
637 of transcriptional variation due to the transient nature of their production. These
638 characteristics are typical of RdDM targets. In contrast, only a few low-expressed genes have
639 at least one of these characteristics in the three different genomic citrus contexts. Generally,
640 RdDM is strongly associated with gene transcriptional repression in *A. thaliana*, maize, tomato
641 and other plant species ((Rymen et al. 2020);(Law et Jacobsen 2010)). However, such a
642 paradigm has been recently challenged by recent studies. In rice, the presence of mCHH on
643 transgenes and endogenous sequences is not always linked to gene repression (Okano et al.
644 2008). In *Poncirus trifoliata*, a close relative of the citrus genus usually used as rootstock,
645 highly expressed genes were more likely to accumulate mCHH sequence contexts in their
646 promoter regions in this species (Wang et al. 2022). The molecular mechanisms that explain
647 the potential involvement of RdDM either in transcriptional repression or activation have
648 been revealed in *A. thaliana*, *via* the identification of different readers of methylated CHH
649 that belong to SUVH histone methyltransferases (Pontvianne et al. 2010). When mCHH is
650 associated with repression, SUVH4, 5 and 6 are recruited. But when mCHH is associated with

651 high expression, SUVH1 and SUVH3 are implicated instead (Harris et al. 2018). These
652 homologs also exist in citrus and are expressed in the parental and the hybrid plants. Creating
653 SUVH1 and SUVH3 methylation reader knock-out using CRISPR-cas9 Should reveal, in the
654 future, if the association is mediated by these specific histone methyltransferases.
655 Furthermore, we could investigate the impact of CHH methylation on highly expressed genes
656 by generating knockouts of essential RdDM core components, such as the *de novo*
657 methyltransferase DRM2 or the catalytic subunit of RNA polymerase V**.** One additional
658 possibility is that open chromatin states and high transcription may favor de novo CHH
659 methylation, as previously observed in chromatin mutants in *Arabidopsis thaliana* (Earley et
660 al. 2010). This hypothesis could be tested by changing the chromatin status of different
661 identified promoter using methylase or demethylase and see how it affects siRNA
662 accumulation and gene expression (Gallego-Bartholomé J. 2020). However, while CRISPR-
663 Cas9 technology is feasible and established protocols exist in citrus (Wang et al. 2023)**,** it
664 remains technically challenging and time-intensive**.** As an alternative approach, we propose
665 to investigate the relationship between CHH methylation patterns and gene expression in
666 citrus under stress conditions or across different developmental stages. This will allow us to
667 assess how these genes respond when their methylation or expression profiles are
668 experimentally altered.
669
670
671 **CONCLUSIONS**
672
673 Our study reveals the impact of DNA methylation and siRNA on the establishment of DEG in
674 a complex inter-specific citrus hybrid. However, additional mechanisms can explain the
675 presence of so many DEG in the hybrid. For example, structural variation including
676 duplication, translocation and inversion contribute to the generated genomic diversity and
677 gene copy number changes that can lead to phenotypic plasticity, including in crops (Picart-
678 Picolo et al. 2020). However, their accurate detection requires a near perfect assembly,
679 usually assisted with chromatin-chromatin interaction maps (Hi-C) approaches which is not
680 our case here.
681 Mobile genetic elements such as transposable elements (TE) can also affect gene expression
682 in two ways: either *via* creating structural variation *via* their neo-insertion, or by modulating
683 gene expression in their vicinity ((Emmerson et Catoni 2025),(Zhang et al. 2023), (Thieme et
684 al. 2022) (Baduel et al. 2019)). Their presence in promoter regions can therefore impact siRNA
685 production and inheritance in hybrid context (Y. Li et al. 2012) . However, in addition to a near
686 perfect assembly, a fine-tuned TE annotation is required in that case and could be the subject
687 of a future study on this hybrid. Finally, mono-allelic expression of certain genes in this
688 complex hybrid may be the consequences of the evolutionary process and the accumulation
689 of genetic and epigenetic modifications in the promoter regions, affecting transcription
690 factors association. Indeed, distant by 4 million years of evolution, the co-evolutionary

691 process between the transcription factors and their targeted regulatory elements in gene
692 promoters may not be fully conserved between the two species.
693
694 In any case, this study proposes an innovative and effective analysis strategy for analysing the
695 molecular consequences of hybridization between distantly related species within the citrus
696 genus. We hope that this strategy will be used in the near future to demonstrate (*i*) the
697 reproducibility of DEG profiles and the impact of DNA methylation and siRNA production in
698 several independent F1 hybrids between these two distantly related species, *C. reticulata* and
699 *C. australasica*, and (*ii*) the ability to combine genomic and epigenomic approaches on young
700 citrus hybrids to anticipate their phenotype during their reproductive stage in terms of their
701 ability to resist pathogens such as Huanglongbing (Graham et al. 2024), but also to produce
702 fruit that meets the standards for marketing.
703
704 **MATERIALS AND METHODS**
705 **Plant material**
706 Hybrid F1 result from a cross between *Citrus reticulata* Blanco cv Fortune mandarin (female
707 parent) and *Citrus australasica* cv Caviar Bachès (Male parent), located at the INRAE CIRAD
708 station in San Giuliano, France. The tissue analysed for *P. trifoliata* and *C. reshni* has been
709 previously described in (Bonnin et al. 2024). The plant material used to analyse *Citrus lemon*
710 and *Citrus sinensis* has been previously described in (Yu et al, 2024) and (Huang et al, 2021)
711 respectively.
712 ***Long-Read Sequencing***
713 Genomic DNA from the hybrid was sequenced using the Oxford Nanopore Technologies (ONT)
714 PromethION platform at the LGDP sequencing facility in Perpignan, generating a total of
715 63.88 Gb of long-read data. This corresponds to approximately 182X coverage of the ~350 Mb
716 genome.
717 **Genome Assembly and Annotation**
718 Nanopore reads from the hybrid were assigned to parental haplotypes using a trio-binning
719 approach. K-mers specific to each parent were extracted from Tell-Seq data using Meryl.
720 Reads were assembled separately for each haplotype using Canu v2.2 (Koren et al. 2017) with
721 options *genomeSize=430m*. Initial polishing of the assemblies was performed using Medaka
722 (Wick 2016), followed by a second round with Pilon (Walker 2014) using the mapped Tell-Seq
723 reads and the options *--fix snps,indels --minmq 3*.
724 **Gene annotation transfer**
725 Gene models were transferred from the reference genomes using Liftoff (Shumate et Salzberg
726 2021) with the parameters *--copies --polish --exclude_partial,* ensuring accurate mapping of
727 complete annotations.
728
729 *Additionnal supporting information can be found in the supplemental material and methods*
730 *document.*
731

ACKNOWLEDGMENTS

The authors would like to thank Raphaël Morillon, Patrick Ollitrault, François Luro, Anne Roulin, Flavia Thiebaut, Marie-Christine Carpentier, Moaine Elbaidouri, Gaëtan Droc, and Gauthier Sarah for fruitful discussions. This work received support from the sequencing and Bioinformatic platforms "Bio-environnement" at the University of Perpignan, the MESO@LR-Platform at the University of Montpellier and technical support from the bioinformatics group of the UMR AGAP Institute, member of the South Green Bioinformatics Platform. We would like to thank the "Occitanie Region" for funding KD and the "Collectivité de Corse" for funding MB. The authors are also grateful to Michel and Benedicte Bachès for sharing leaves to analyse the parental line *C. australasica.*

CONTRIBUTIONS

A. G. performed the statistical modelling presented in FIG 5C-F. Y. F. created the citrus hybrid. K. D. extracted the RNA and DNA from the parent and the hybrid with the help of N. P. and F.P. M.B. realised RNA-seq and WGBS analyses for *C. reshni* and *P. trifoliata*. C.L. performed nanopore sequencing. F.P., N.P. and B. H. conceived and designed all experiments. K. D. performed all bioinformatic analyses with some help of M-C.C and N.P. and B.H. F.P. wrote the article with substantial contributions of K.D., B.H and A. G.. N.P. edited the article. N.P. and F.P. acquired main funding. F.P., N.P. and B.H. coordinated the research. All authors approved submission. All authors have read and agreed to the published version of the manuscript.

DATA AVAILABILITY STATEMENT

Nucleotide sequencing data generated in this study have been deposited in European Nucleotide Archive (ENA) under the accession number PRJEB94133 (https://www.ebi.ac.uk/ena/browser/search/PRJEB94133).

FUNDING

KD is supported by a PhD fellowship from Allocation Doctorale Occitanie (2022-25 Save-Citrus) and the Doctoral school ED 305 from UPVD. MB was funded by the "Collectivité de Corse" and CIRAD Montpellier UMR AGAP Team Seapag and Team MEAC at LGDP. This work was mainly supported by the UPVD (BQR-2022). This study was also supported by the Laboratoires d'Excellence (LABEX) TULIP (ANR-10-LABX-41) and by the École Universitaire de Recherche (EUR) TULIP-GS (ANR-18-EURE-0019). BH work was supported by the French National Research Agency (ANR) under Grant ANR-23-CE20-0038.

CONFLICT OF INTERESTS

The authors declare no competing interest.

773 **REFERENCES**

774

775

776 Al-Khayri. 2018. *Advances in Plant Breeding Strategies: Fruits*. https://doi.org/10.1007/978-
777 3-319-91944-7.

778 Alquézar, Berta, Lourdes Carmona, Stefania Bennici, Marcelo P. Miranda, Renato B. Bassanezi,
779 et Leandro Peña. 2022. « Cultural Management of Huanglongbing: Current Status and
780 Ongoing Research ». *Phytopathology* 112 (1): 11-25. https://doi.org/10.1094/PHYTO-
781 08-21-0358-IA.

782 Alves, Mônica N., Laudecir L. Raiol-Junior, Eduardo A. Girardi, et al. 2022. « Insight into
783 Resistance to 'Candidatus Liberibacter Asiaticus,' Associated with Huanglongbing, in
784 Oceanian Citrus Genotypes ». *Frontiers in Plant Science* 13 (septembre).
785 https://doi.org/10.3389/fpls.2022.1009350.

786 Baduel, Pierre, Leandro Quadrana, Ben Hunter, Kirsten Bomblies, et Vincent Colot. 2019.
787 « Relaxed Purifying Selection in Autopolyploids Drives Transposable Element Over-
788 Accumulation Which Provides Variants for Local Adaptation ». *Nature*
789 *Communications* 10 (1): 5818. https://doi.org/10.1038/s41467-019-13730-0.

790 Birchler, James A., Hong Yao, Sivanandan Chudalayandi, Daniel Vaiman, et Reiner A. Veitia.
791 2010. « Heterosis ». *The Plant Cell* 22 (7): 2105-12.
792 https://doi.org/10.1105/tpc.110.076133.

793 Bonnin M *et al.* Comparative transcriptomic analyses of diploid and tetraploid citrus reveal
794 how ploidy level influences salt stress tolerance. *Front Plant Sci* 2024; **15**: 1469115.

795 Cimen, Berken, Turgut Yesiloglu, Bilge Yilmaz, et Meral Incesu. 2022. « Genetic Improvement
796 in Citrus ». In *Citrus Production*. CRC Press.

797 Costa, Gustavo Vaz da, Carmen Silvia Vieira Janeiro Neves, Renato Beozzo Bassanezi, Rui
798 Pereira Leite Junior, et Tiago Santos Telles. 2021. « Economic Impact of Huanglongbing
799 on Orange Production ». *Revista Brasileira de Fruticultura* 43 (juin): e.
800 https://doi.org/10.1590/0100-29452021472.

801 Curk, Franck, François Luro, Sajjad Hussain, et Patrick Ollitrault. 2022. « Citrus Origins ». In
802 *Citrus Production*. CRC Press.

803 Dahro, Bachar, Chunlong Li, et Ji-Hong Liu. 2023. « Overlapping Responses to Multiple Abiotic
804 Stresses in Citrus: From Mechanism Understanding to Genetic Improvement ».
805 *Horticulture Advances* 1 (1): 4. https://doi.org/10.1007/s44281-023-00007-2.

806 Droc, Gaetan, Delphine Giraud, Caroline Belser, et al. 2024. « A Super-Pangenome for
807 Cultivated Citrus Reveals Evolutive Features during the Allopatric Phase of Their
808 Reticulate Evolution ». Prépublication, bioRxiv, octobre 18.
809 https://doi.org/10.1101/2024.10.17.618847.

810 Earley Keith W., Pontvianne Frederic, Wierzbicki Andrzej, *et al.* « Mechanisms of HDA6-
811 mediated rRNA gene silencing : suppression of intergenic Pol II transcription and
812 differential effects on maintenance versus siRNA-directed cytosine methylation ».
813 *Genes Dev* 2010; **24**: 1119–1132.

814 Emmerson, Robyn, et Marco Catoni. 2025. « The role of mobile DNA elements in the dynamic
815 of plants genome plasticity ». *Journal of Experimental Botany*, n° erae523 (janvier).
816 https://doi.org/10.1093/jxb/erae523.

817 Gallego-Bartolomé J. 2020. « DNA methylation in plants: mechanisms and tools for targeted
818 manipulation ». *New Phytol*. Jul;227(1):38-44. doi: 10.1111/nph.16529.

819 Giraud, Delphine, Nathalie Choisne, Marilyne Summo, et al. 2025. « Construction of a
820 comprehensive library of repeated sequences for the annotation of Citrus genomes ».
821 *BMC Genomic Data* 26 (1): 30. https://doi.org/10.1186/s12863-025-01321-6.
822 Graham, James H., Renato B. Bassanezi, William O. Dawson, et Rick Dantzler. 2024.
823 « Management of Huanglongbing of Citrus: Lessons from São Paulo and Florida ».
824 *Annual Review of Phytopathology* 62 (Volume 62, 2024): 243-62.
825 https://doi.org/10.1146/annurev-phyto-121423-041921.
826 Greaves, Ian K., Rebeca Gonzalez-Bayon, Li Wang, et al. 2015. « Epigenetic Changes in
827 Hybrids ». *Plant Physiology* 168 (4): 1197-205. https://doi.org/10.1104/pp.15.00231.
828 Greaves, Ian K., Michael Groszmann, Hua Ying, Jennifer M. Taylor, W. James Peacock, et
829 Elizabeth S. Dennis. 2012. « Trans Chromosomal Methylation in Arabidopsis hybrids ».
830 *Proceedings of the National Academy of Sciences* 109 (9): 3570-75.
831 https://doi.org/10.1073/pnas.1201043109.
832 Harris, C. Jake, Marion Scheibe, Somsakul Pop Wongpalee, et al. 2018. « A DNA Methylation
833 Reader Complex That Enhances Gene Transcription ». *Science (New York, N.Y.)* 362
834 (6419): 1182-86. https://doi.org/10.1126/science.aar7854.
835 He, Li, Cheng Zhao, Qingzhu Zhang, et al. 2021. « Pathway conversion enables a double-lock
836 mechanism to maintain DNA methylation and genome stability ». *Proceedings of the*
837 *National Academy of Sciences* 118 (35): e2107320118.
838 https://doi.org/10.1073/pnas.2107320118.
839 Hochholdinger, Frank, et Peng Yu. 2025. « Molecular Concepts to Explain Heterosis in Crops ».
840 *Trends in Plant Science* 30 (1): 95-104. https://doi.org/10.1016/j.tplants.2024.07.018.
841 Huang Y *et al.* Genome of a citrus rootstock and global DNA demethylation caused by
842 heterografting. *Hortic Res* 2021; **8**: 69.
843 Kakoulidou, Ioanna, et Frank Johannes. 2024. « DNA Methylation Remodeling in F1 Hybrids ».
844 *The Plant Journal: For Cell and Molecular Biology* 118 (3): 671-81.
845 https://doi.org/10.1111/tpj.16137.
846 Kakoulidou, Ioanna, Robert S. Piecyk, Rhonda C. Meyer, et al. 2024. « Mapping Parental DMRs
847 Predictive of Local and Distal Methylome Remodeling in Epigenetic F1 Hybrids ».
848 Research Articles. *Life Science Alliance* 7 (4). https://doi.org/10.26508/lsa.202402599.
849 Koren, Sergey, Arang Rhie, Brian P. Walenz, et al. 2018. « De Novo Assembly of Haplotype-
850 Resolved Genomes with Trio Binning ». *Nature Biotechnology* 36 (12): 1174-82.
851 https://doi.org/10.1038/nbt.4277.
852 Koren, Sergey, Brian P. Walenz, Konstantin Berlin, Jason R. Miller, Nicholas H. Bergman, et
853 Adam M. Phillippy. 2017. « Canu: scalable and accurate long-read assembly via
854 adaptive k-mer weighting and repeat separation ». *Genome Research* 27 (5): 722-36.
855 https://doi.org/10.1101/gr.215087.116.
856 Lauss, Kathrin, René Wardenaar, Rurika Oka, et al. 2018. « Parental DNA Methylation States
857 Are Associated with Heterosis in Epigenetic Hybrids ». *Plant Physiology* 176 (2):
858 1627-45. https://doi.org/10.1104/pp.17.01054.
859 Law, Julie A., et Steven E. Jacobsen. 2010. « Establishing, Maintaining and Modifying DNA
860 Methylation Patterns in Plants and Animals ». *Nature Reviews Genetics* 11 (3): 204-20.
861 https://doi.org/10.1038/nrg2719.
862 Li, Heng. 2018. « Minimap2: pairwise alignment for nucleotide sequences ». *Bioinformatics*
863 34 (18): 3094-100. https://doi.org/10.1093/bioinformatics/bty191.
864 Li, Ying, Kranthi Varala, Stephen P. Moose, et Matthew E. Hudson. 2012. « The Inheritance
865 Pattern of 24 Nt siRNA Clusters in Arabidopsis Hybrids Is Influenced by Proximity to

Transposable Elements ». *PLOS ONE* 7 (10): e47043. https://doi.org/10.1371/journal.pone.0047043.

Mahmoud, Lamiaa M., et Manjul Dutt. 2025. « Novel Citrus Hybrids Incorporating Australian Lime Genetics: Development of HLB-Tolerant Citrus Rootstocks and Physiological Changes in 'Valencia' Sweet Orange Scions ». *Frontiers in Plant Science* 16 (juin). https://doi.org/10.3389/fpls.2025.1614845.

Martin, Guillaume, Franc-Christophe Baurens, Gaëtan Droc, et al. 2016. « Improvement of the banana "Musa acuminata" reference sequence using NGS data and semi-automated bioinformatics methods ». *BMC Genomics* 17 (1): 243. https://doi.org/10.1186/s12864-016-2579-4.

Mason, Annaliese S., et Jacqueline Batley. 2015. « Creating New Interspecific Hybrid and Polyploid Crops ». *Trends in Biotechnology* 33 (8): 436-41. https://doi.org/10.1016/j.tibtech.2015.06.004.

Matzke, Marjori A., Tatsuo Kanno, et Antonius J. M. Matzke. 2015. « RNA-Directed DNA Methylation: The Evolution of a Complex Epigenetic Pathway in Flowering Plants ». *Annual Review of Plant Biology* 66: 243-67. https://doi.org/10.1146/annurev-arplant-043014-114633.

MUKHAMETZYANOV, R. R., S. V. BRUSENKO, A. M. KHEZHEV, E. M. KELEMETOV et S. S.KIRILLOVA (2024). "Changing the Global Production and Trade of Citrus Fruits". In : Sus-tainable Development of the Agrarian Economy Based on Digital Technologies and Smart Innova-tions. Sous la dir. d'E. G. POPKOVA, A. V. BOGOVIZ, B. S. SERGI, O. V. KAUROVA et A. N.MALOLETKO. Cham : Springer Nature Switzerland, p. 19-24. ISBN : 978-3-031-51272-8.

Nakandala, Upuli, Agnelo Furtado, Malcolm W. Smith, et al. 2023. « Phylogenetic Relationships among Australian Native Citrus Species Based upon Complete Chloroplast Genomes and Single Copy Nuclear Genes ». *Tropical Plants* 2 (1): TP-2023-0021. https://doi.org/10.48130/TP-2023-0021.

Okano, Yosuke, Daisuke Miki, et Ko Shimamoto. 2008. « Small Interfering RNA (siRNA) Targeting of Endogenous Promoters Induces DNA Methylation, but Not Necessarily Gene Silencing, in Rice ». *The Plant Journal* 53 (1): 65-77. https://doi.org/10.1111/j.1365-313X.2007.03313.x.

Ollitrault, Patrick, Franck Curk, et Robert Krueger. 2020. « Citrus Taxonomy ». In *The Genus Citrus*. Elsevier. https://doi.org/10.1016/B978-0-12-812163-4.00004-8.

Ollitrault, Patrick, Barbara Hufnagel, Franck Curk, et al. 2024. « Comparative Genetic Mapping and a Consensus Interspecific Genetic Map Reveal Strong Synteny and Collinearity within the Citrus Genus ». *Frontiers in Plant Science* 15 (décembre). https://doi.org/10.3389/fpls.2024.1475965.

Peng, Ze, Jessen V. Bredeson, Guohong A. Wu, et al. 2020. « A chromosome-scale reference genome of trifoliate orange (Poncirus trifoliata) provides insights into disease resistance, cold tolerance and genome evolution in Citrus ». *The Plant Journal* 104 (5): 1215-32. https://doi.org/10.1111/tpj.14993.

Picart-Picolo, Ariadna, Stefan Grob, Nathalie Picault, et al. 2020. « Large Tandem Duplications Affect Gene Expression, 3D Organization, and Plant-Pathogen Response ». *Genome Research* 30 (11): 1583-92. https://doi.org/10.1101/gr.261586.120.

Pontvianne, Frédéric, Todd Blevins, et Craig S. Pikaard. 2010. « Arabidopsis Histone Lysine Methyltransferases ». In *Advances in Botanical Research*, édité par Jean-Claude Kader et Michel Delseny, vol. 53. Advances in Botanical Research. Academic Press.

https://doi.org/10.1016/S0065-2296(10)53001-5.
Rymen, Bart, Laura Ferrafiat, et Todd Blevins. 2020. « Non-Coding RNA Polymerases That Silence Transposable Elements and Reprogram Gene Expression in Plants ». *Transcription* 11 (3-4): 172-91. https://doi.org/10.1080/21541264.2020.1825906.
Shumate, Alaina, et Steven L. Salzberg. 2021. « Liftoff: Accurate Mapping of Gene Annotations ». *Bioinformatics (Oxford, England)* 37 (12): 1639-43. https://doi.org/10.1093/bioinformatics/btaa1016.
Stroud, Hume, Truman Do, Jiamu Du, et al. 2014. « Non-CG Methylation Patterns Shape the Epigenetic Landscape in Arabidopsis ». *Nature Structural & Molecular Biology* 21 (1): 64-72. https://doi.org/10.1038/nsmb.2735.
Thieme, Michael, Arthur Brêchet, Yann Bourgeois, Bettina Keller, Etienne Bucher, et Anne C. Roulin. 2022. « Experimentally heat-induced transposition increases drought tolerance in Arabidopsis thaliana ». *The New Phytologist* 236 (1): 182-94. https://doi.org/10.1111/nph.18322.
Walker, Bruce J. 2014. « Pilon: An Integrated Tool for Comprehensive Microbial Variant Detection and Genome Assembly Improvement | PLOS One ». https://journals.plos.org/plosone/article?id=10.1371/journal.pone.0112963.
Wang, Min, Yang-Yang Qin, Nan-Nan Wei, Huan-Ying Xue, Wen-Shan Dai. 2023 « Highly efficient *Agrobacterium rhizogenes*-mediated hairy root transformation in citrus seeds and its application in gene functional analysis. » *Front Plant Sci.* Oct 31;14:1293374. doi: 10.3389/fpls.2023.1293374.
Wang, Yue, Lanlan Zuo, Tonglu Wei, et al. 2022. « CHH Methylation of Genes Associated with Fatty Acid and Jasmonate Biosynthesis Contributes to Cold Tolerance in Autotetraploids of Poncirus Trifoliata ». *Journal of Integrative Plant Biology* 64 (12): 2327-43. https://doi.org/10.1111/jipb.13379.
Wick, Ryan. (2016) 2025. *rrwick/Unicycler*. C++. mars 14, released juin 14. https://github.com/rrwick/Unicycler.
Wu, Guohong Albert, Javier Terol, Victoria Ibanez, et al. 2018. « Genomics of the Origin and Evolution of Citrus ». *Nature* 554 (7692): 311-16. https://doi.org/10.1038/nature25447.
Xia, Qiang-Ming, Lu-Ke Miao, Kai-Dong Xie, et al. 2020. « Localization and Characterization of Citrus Centromeres by Combining Half-Tetrad Analysis and CenH3-Associated Sequence Profiling ». *Plant Cell Reports* 39 (12): 1609-22. https://doi.org/10.1007/s00299-020-02587-z.
Yesiloglu, Turgut, Bilge Yilmaz, Meral Incesu, et Berken Çimen. 2022. *Challenges to the Citrus Industry*. https://doi.org/10.1201/9781003119852-2.
Yu H *et al.* The lemon genome and DNA methylome unveil epigenetic regulation of citric acid biosynthesis during fruit development. *Hortic Res* 2024; **11**: uhae005.
Zhan, Junpeng, et Blake C. Meyers. 2023. « Plant Small RNAs: Their Biogenesis, Regulatory Roles, and Functions ». *Annual Review of Plant Biology* 74 (Volume 74, 2023): 21-51. https://doi.org/10.1146/annurev-arplant-070122-035226.
Zhang, Panpan, Assane Mbodj, Abirami Soundiramourtty, et al. 2023. « Extrachromosomal Circular DNA and Structural Variants Highlight Genome Instability in Arabidopsis Epigenetic Mutants ». *Nature Communications* 14 (1): 5236. https://doi.org/10.1038/s41467-023-41023-0.

Supplemental Figures and Tables

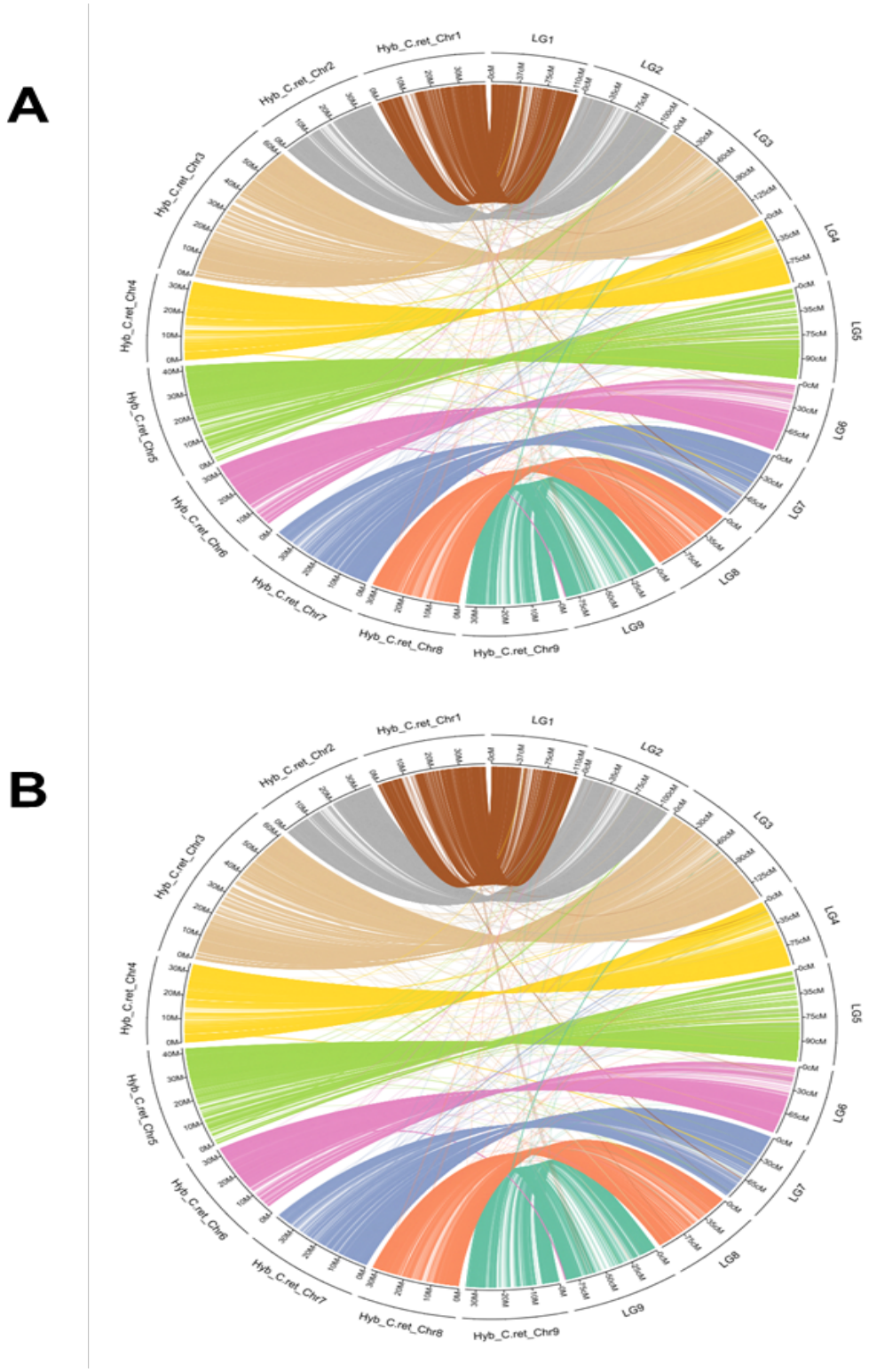

Figure S1. Anchoring of the haplotype assemblies to the consensus Citrus genetic map. *Each ribbon connects a genomic scaffold from the haplotype assembly (left) to its corresponding position in one of the nine linkage groups (right). (**A**) Haplotype derived from C. reticulata. (**B**) Haplotype derived from C. australasica. The strong one-to-one correspondence and limited cross-linking support the structural accuracy of the assemblies.*

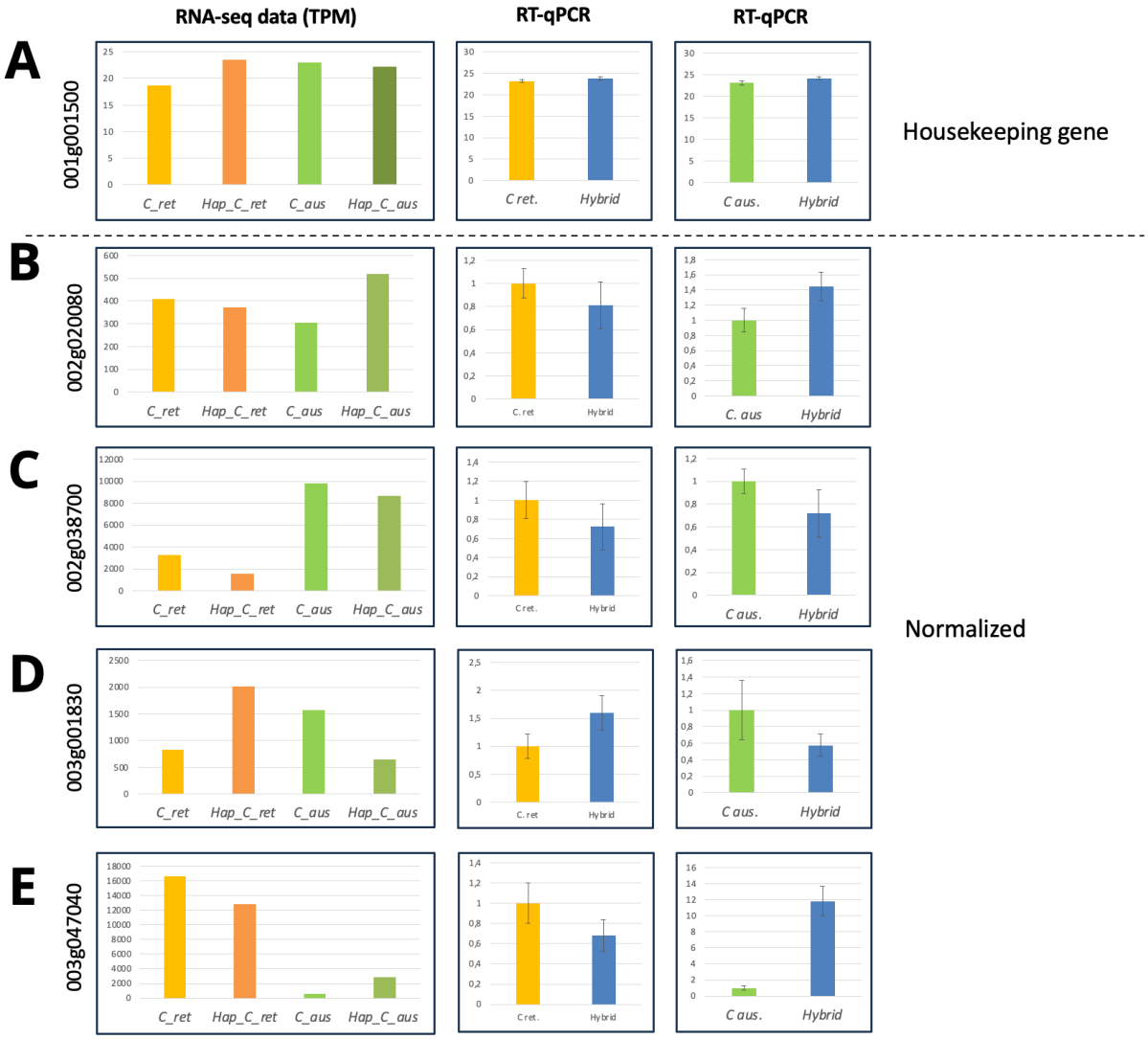

Figure S2. Validation of RNA-seq analyses by RT-qPCR.

*Analyses of transcripts accumulation of five different expressed genes in the parental and the hybrid lines according to the RNA-seq analyses (left graphic) or by RT-qPCR using C. reticulata-specific primers (middle praphic) or C. australasica-specific primers (right graphics). RT-qPCR of genes presented in the panel **B-D** were normalized according the housekeeping gene encoding UBIQUITIN (panel **A**; 001g001500).*

A Hyb *C. aus* REVIGO TreeMaps of enriched Biological Process (GO)

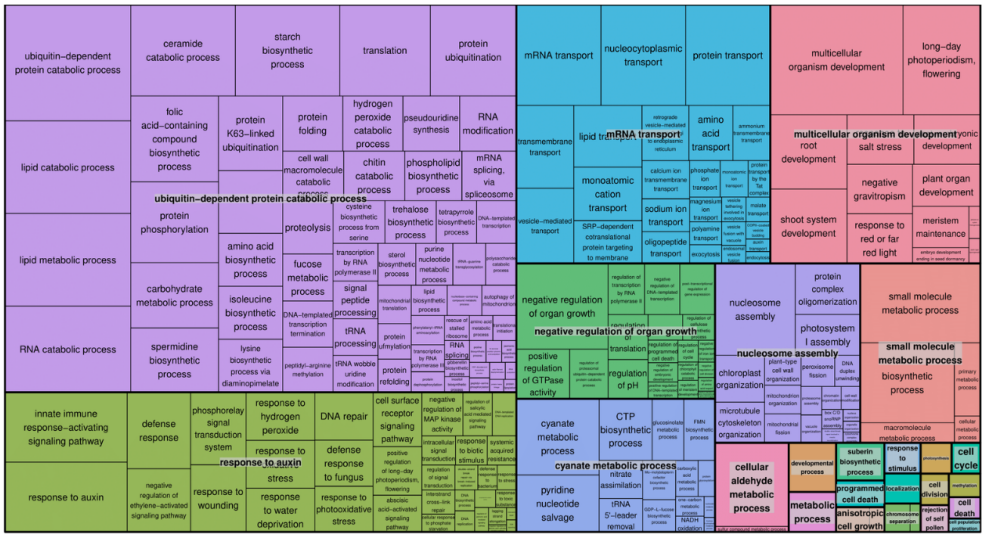

B Hyb *C. ret* REVIGO TreeMaps of enriched Biological Process (GO)

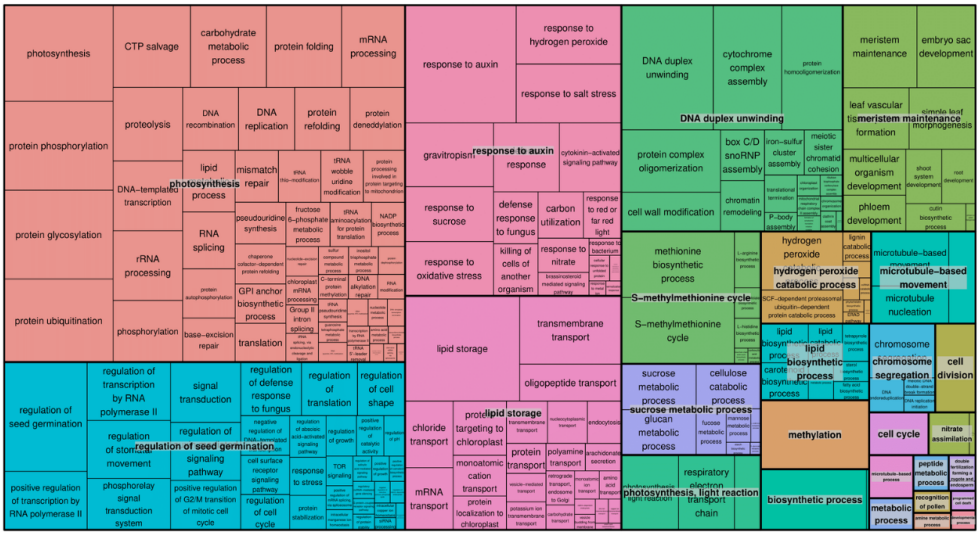

Figure S3. REVIGO TreeMaps of enriched Biological Process (GO) terms among differentially expressed genes (DEGs) in the hybrid.

(A) *GO terms enriched among genes upregulated from the C. australasica haplotype. Major categories include ubiquitin-dependent protein catabolic process, protein catabolic/metabolic process, translation, RNA modification and transport, and stress and defence responses.* ***(B)*** *GO terms enriched among genes upregulated from the C. reticulata haplotype. Enriched categories include photosynthesis, protein phosphorylation, RNA processing, DNA replication, NADP biosynthetic process, and other central metabolic and transcriptional functions, indicating a predominant maternal contribution to core cellular activities.*

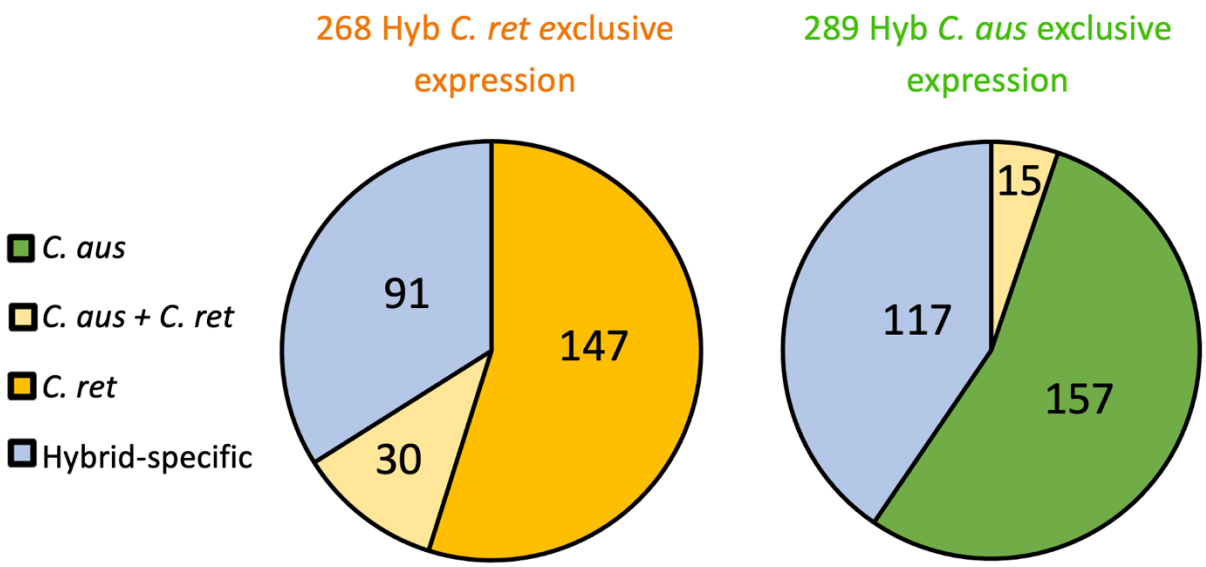

Figure S4. Exclusive allelic expression in the hybrid.

Pie-chart diagram showing the origin of the allele exclusively expressed by the C. australasica haplotype (right) or the C. reticulata haplotype (left) in the hybrid. These genes are then separated in four categories: those that are only expressed in the hybrid and not in the parental lines (Hybrid-specific; blue), those that are also expressed in C. australasica (C. aus; green) or in C. reticulata (C. ret; orange) parental lines and those that are expressed in both parents (C. aus + C. ret; beige colour).

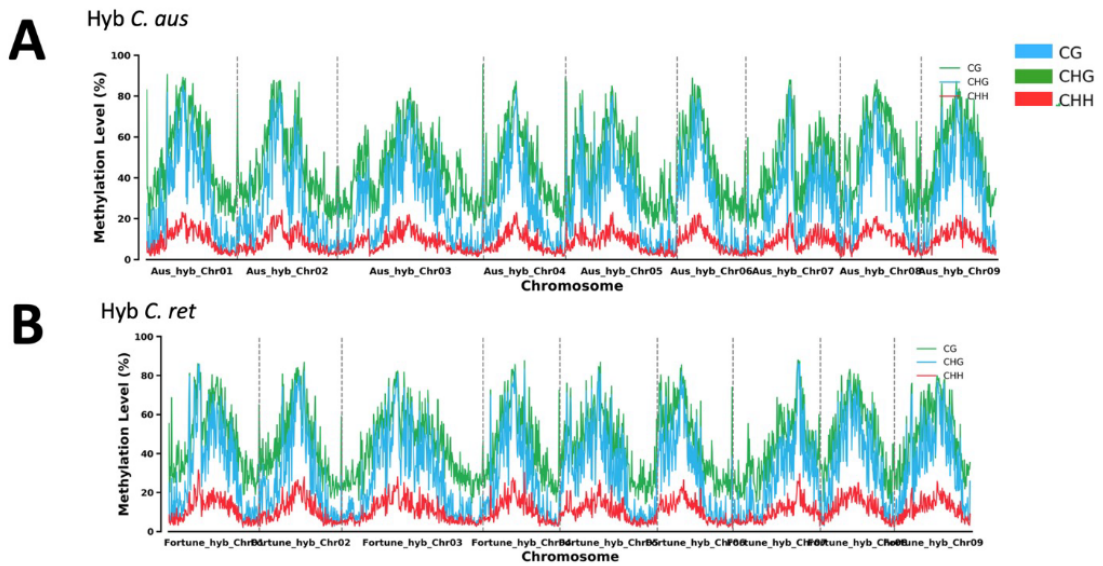

Figure S5. Genomic distribution of DNA methylation in the hybrid.

*The distribution of the three DNA methylation patterns (CG, CHG and CHH) is shown across all haplotype resolved hybrid C. aus (**A**) or hybrid C. ret. (**B**) chromosomes.*

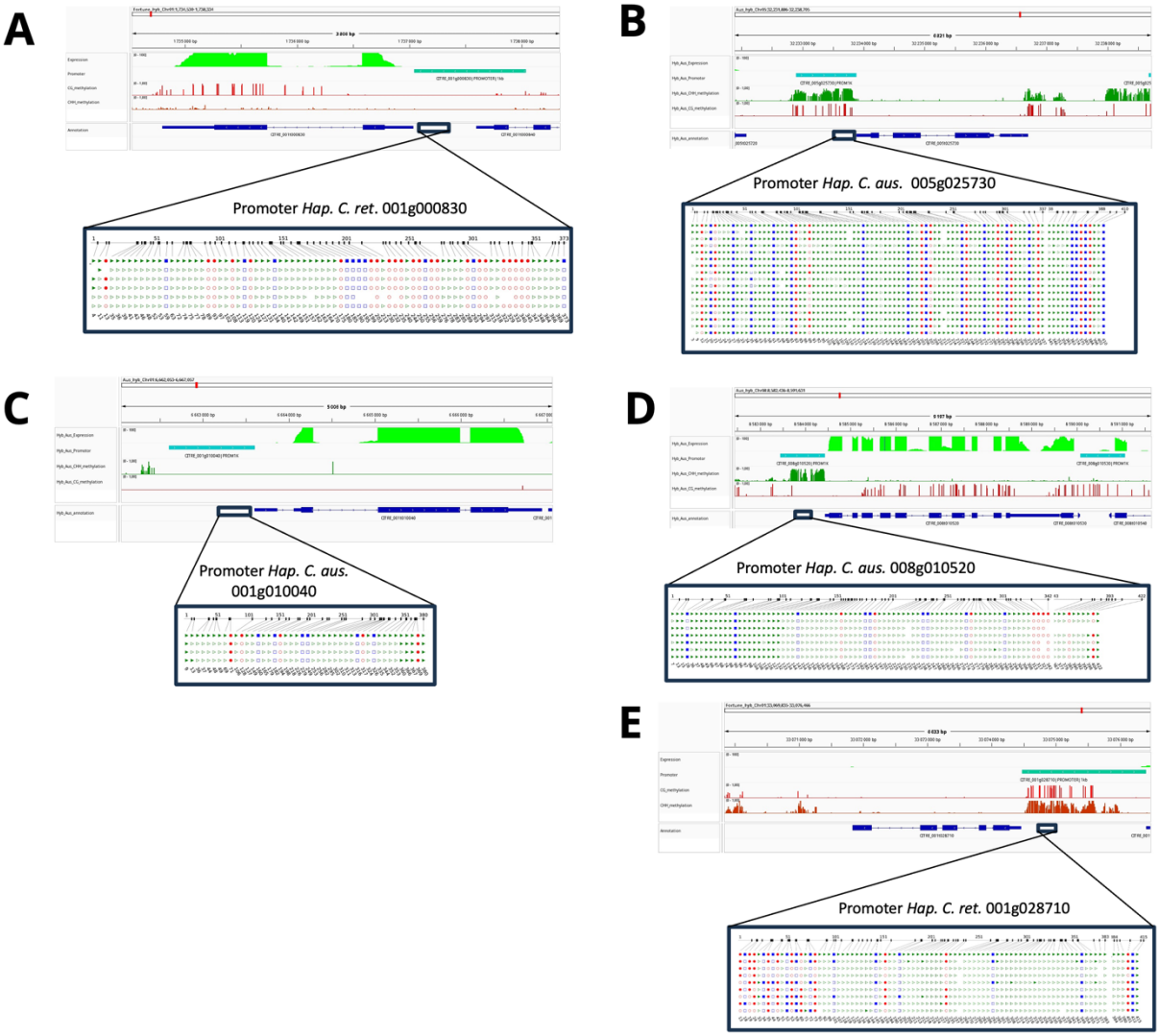

Figure S6. WGBS validation using BS-PCR and Sanger sequencing

*To validate the methylation profiles obtained by WGBS, we designed primers at five different genomic location, performed bisulfite treatment and amplified selected promoter regions using specific primers. Browser screenshot displays the data obtained using WGBS and RNA-seq data, separating CHH and CG methylation. The black square corresponds to the genomic location amplified by PCR, cloned and sequenced using Sanger technic. Methylation analyses were then performed using CYMATE (www.cymate.org). As expected, unmethylated promoter regions in WGBS are also unmethylated when analysed by BS-PCR (**A**, **C**), while methylated promoter regions accumulate methylation in CHH context only (**D**), or at both CG and CHH context (**B**, **E**).*

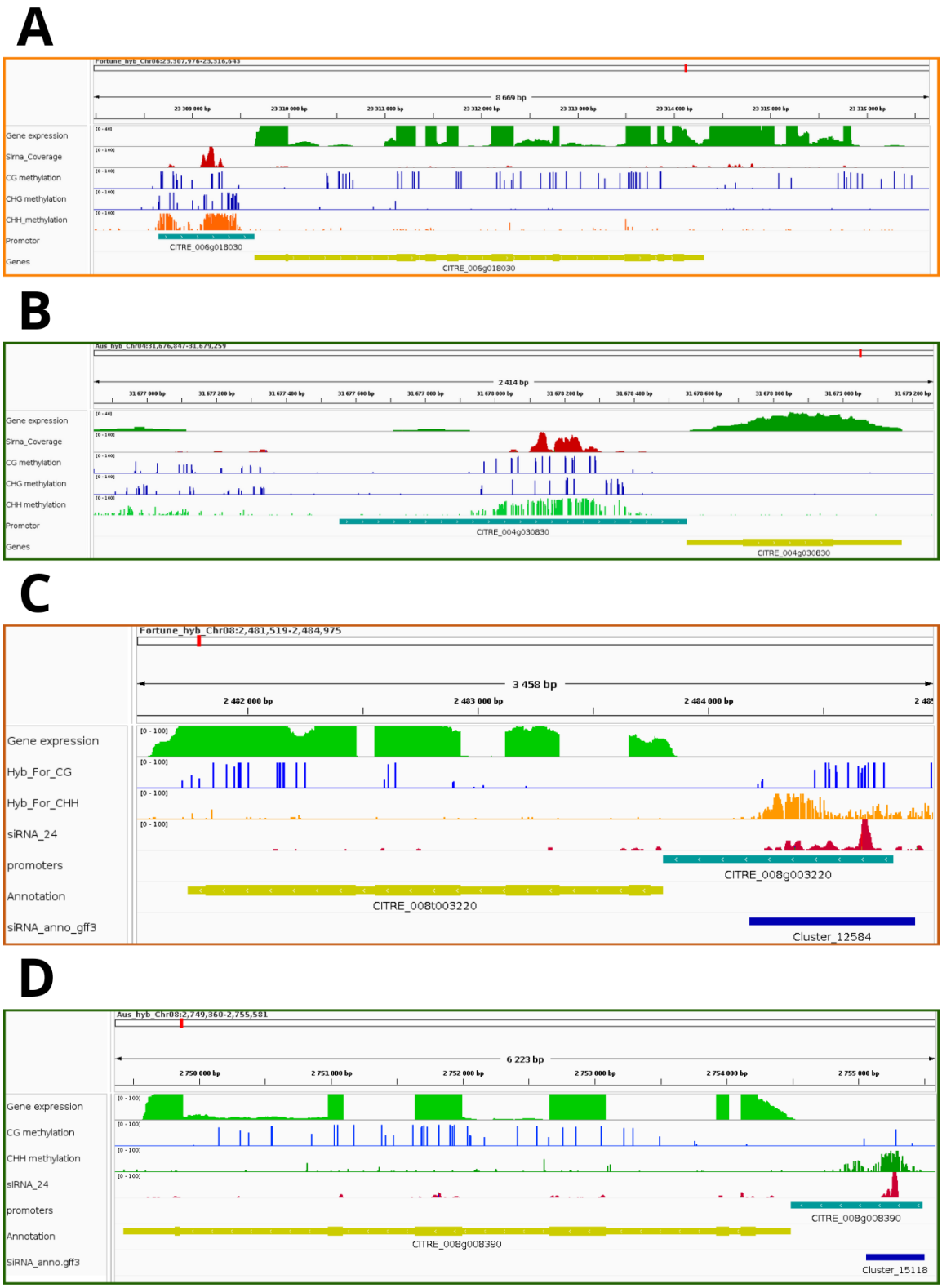

Figure S7. screenshot of IGV browser.

*IGV screenshot examples showing the distribution of small RNA clusters, mRNA accumulation, and CG or CHH methylation accumulation along 4 genomic loci in the hyb C. ret (**A, C**) or Hyb C. aus (**B, D**). In these 4 cases, the presence of siRNA clusters and mCHH in the promoter regions is not incompatible with gene expression.*

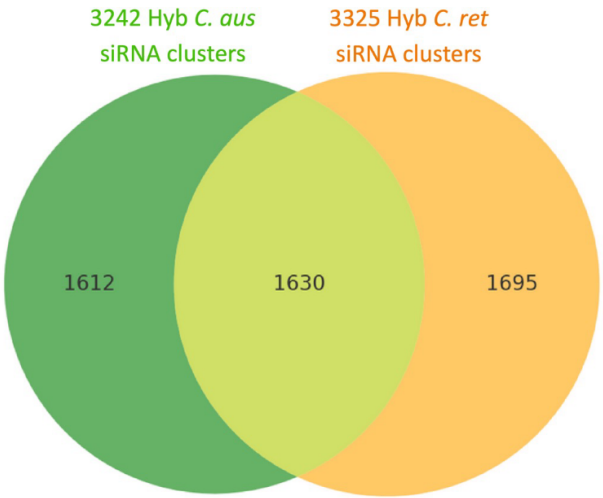

Figure S8. SiRNA clusters in the hybrid.

Venn diagram showing the overlap of unique 24-nt siRNA sequences identified from clusters annotated independently in each haplotype (C. reticulata and C. australasica). About one third of 24-nt siRNA sequences (1630) are shared between the two haplotypes, while the remaining sequences are unique to one or the other: 1612 being specific to C. australasica haplotype (left, green), and 1695 being specific to the C. reticulata (right, orange) haplotype.

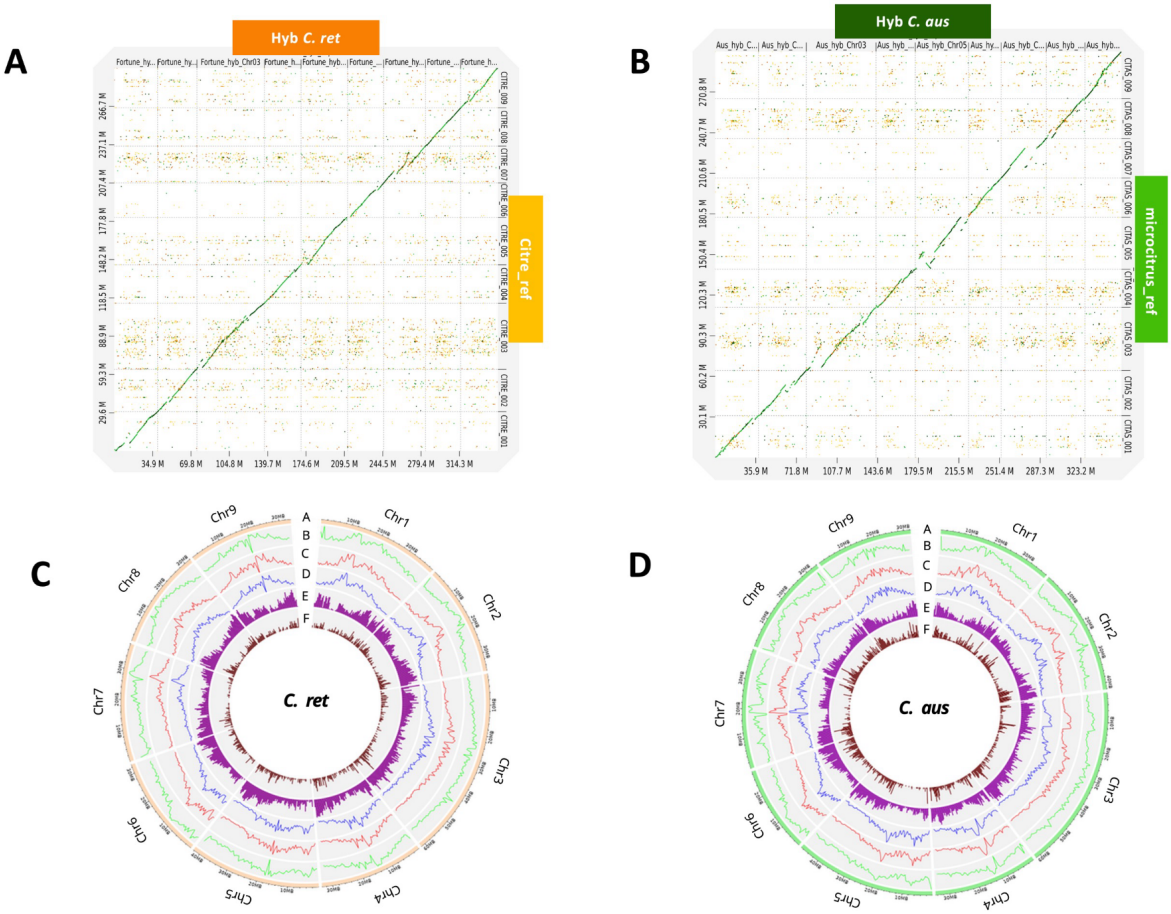

Figure S9. Genome-wide epigenomic patterns and overlap with expression in the parental lines.

*(**A**) Dot-plot alignment between the maternal haplotype of the hybrid C. ret and CITRE reference. (**B**) Dot-plot alignment between the paternal haplotype hybrid C. aus and the C. australasica reference genome. These plots illustrate overall synteny and structural rearrangements between each haplotype of the hybrid and the closest available reference genome from the corresponding parental line. Diagonal lines indicate conserved homologous regions, while off-diagonal signals highlight structural variations. (**C–D**) Circos plots representing genome-wide profiles of DNA methylation, gene density, and 24-nt siRNA clusters across the nine chromosomes of the two parental lines C. reticulata (**C**) and C. australasica (**D**).*

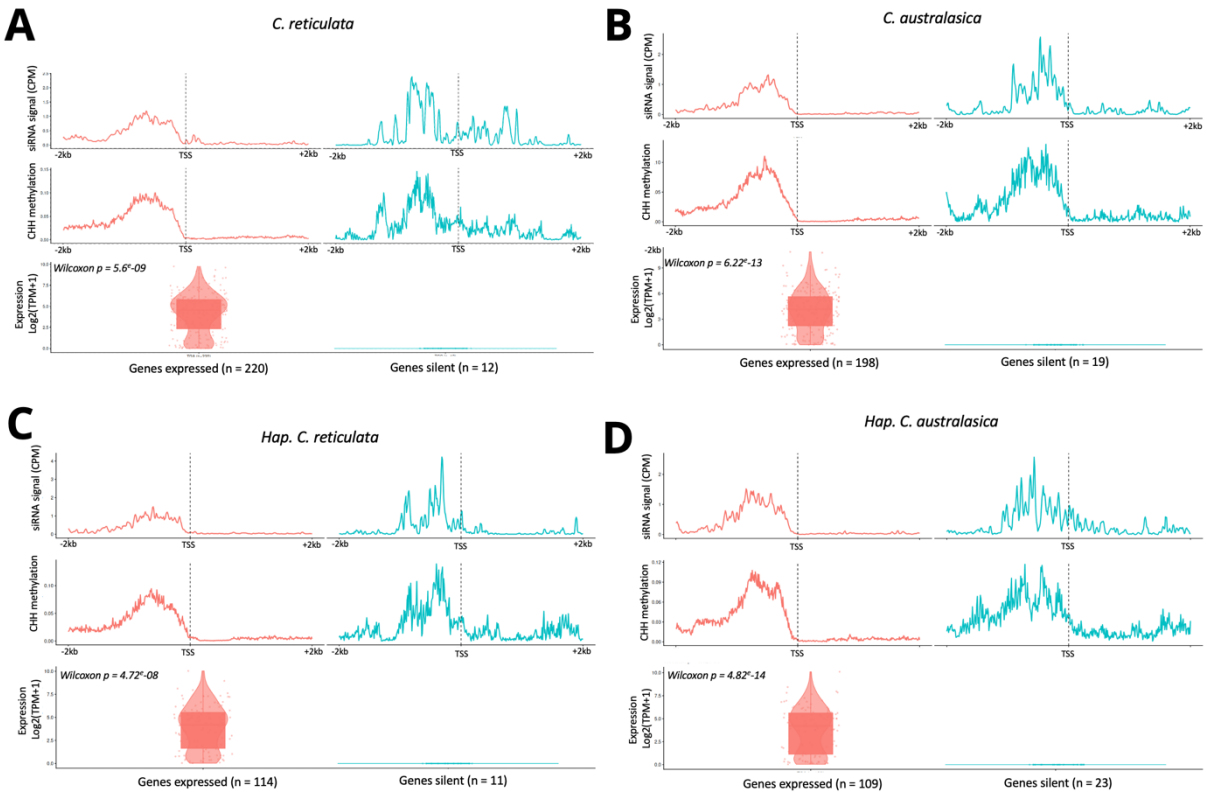

Figure S10. Specific analyses of siRNA–CHH methylation–gene expression modules in the C. ret, C. aus and in the hybrid.

*Metagene plots displaying 24-nt siRNA accumulation (top), CHH methylation (middle panel) and gene expression of siRNA–CHH methylation–gene modules with expressed genes (left panel) or silent genes (right panel) in C. reticulata (**A**), in C. australasica (**B**), or in the hybrid with an haplotype resolution (**C-D**). Metagene plots displays the accumulation from -2kb to +2kb of the Transcription start site (TSS).*

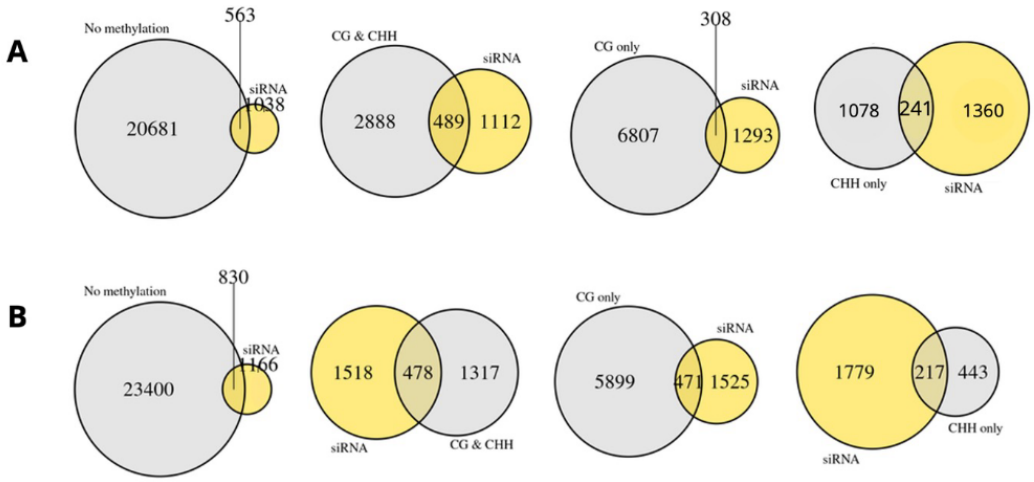

Figure S11. Venn diagrams showing the overlap between siRNA presence and methylation categories in parental genomes.

*Each plot displays the number of genes in a given methylation class (grey) and those with 24-nt siRNA clusters in their promoters (yellow) in C. reticulata (**A**) or in C. australasica (**B**). Overlaps represent genes with both features. Separate diagrams are shown for each methylation category.*

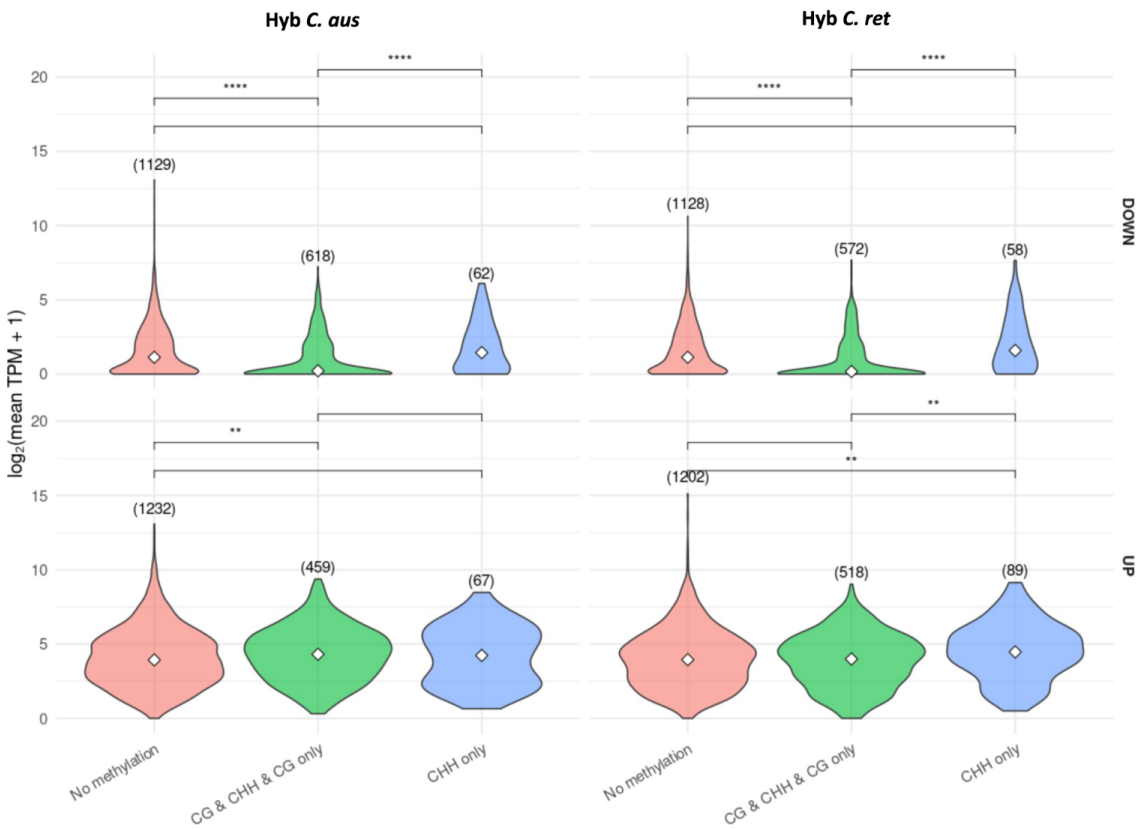

Figure S12. DNA methylation associating with the promoter of DEG in the hybrid

Violin plots displaying the distribution of DEG genes for each haplotype according to the type of methylation accumulating in their promoter regions. CHH > 20%; CG > 40%.

A

Genes	Citrus_gene_id	*C. Reticulata*	*Hap. C. ret.*	*C. australasi*	*Hap. C. aus.*
NRPD1	CITRE_003g011380	4,767334	4,29413733	2,158684	1,429438
NRPE1	CITRE_008g018100	11,3111357	10,2296567	13,6122613	15,0771083
DRM2	CITRE_002g008120	27,0843727	41,0615447	25,4039753	30,5621017
AGO4	CITRE_002g006780	164,122676	155,941335	130,161471	124,150246
AGO6	CITRE_002g020700	7,006687	7,03087667	4,41796067	3,92255767
SUVH4/KYP	CITRE_002g012110	13,5418107	19,1116547	9,62826167	10,1865453
SUVH6	CITRE_005g013450	39,1862233	39,4222197	40,0289423	41,050663
MET1	CITRE_007g009140	1,88593033	1,90298567	1,343297	3,34992833
CMT3	CITRE_002g001610	0,94181633	1,84237067	1,16343533	0,95102667
CMT2	CITRE_005g014740	0,978142	2,56786967	16,1104	18,615868
DDM1	CITRE_007g003580	1,08242133	1,89476467	1,29368567	1,48642333

B

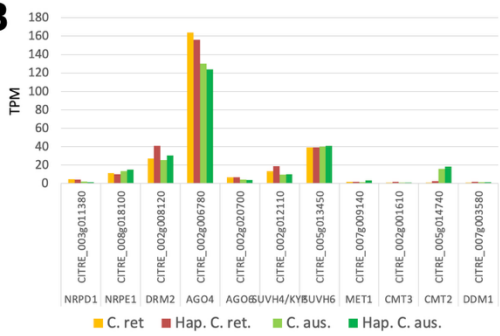

Figure S13. Relative expression of RdDM members in the hybrid and the parent

*Analyses of the relative expression levels of several major homologs of the RdDM in the hybrid haplotypes and in the parental lines. Data were extracted from the RNA-seq and are presented as table (**A**) and in the graphic (**B**). TPM =* Transcripts Per Kilobase Million

Sample	Raw Reads	Trimmed Reads	Mapped Reads	Total Mapped (%)
Hyb_C.ret_rep1	31,570,252	29,619,476	29,179,963	98.51
Hyb_C.ret_rep2	31,149,835	29,499,214	29,085,818	98.57
Hyb_C.ret_rep3	31,411,499	29,720,267	29,294,474	98.57
*C. reticulata*_rep1	31,136,378	29,435,073	28,976,206	98.44
*C. reticulata*_rep2	32,938,492	31,231,204	30,636,695	98.09
*C. reticulata*_rep3	31,448,963	29,651,782	29,120,932	98.21
*C. australasica*_rep1	28,905,022	27,272,835	26,792,030	98.24
*C. australasica*_rep2	31,215,753	29,470,075	28,936,627	98.19
*C. australasica*_rep3	30,971,028	29,478,682	28,978,279	98.30
Hyb_C.aus_rep1	31,570,252	29,619,476	29,254,611	98.77
Hyb_C.aus_rep1	31,149,835	29,499,214	29,164,128	98.86
Hyb_C.aus_rep1	31,411,499	29,720,267	29,367,248	98.81

Table S1. Summary of RNA-seq data processing and mapping.

This table presents, for each replicate, the total number of raw reads, the number of reads retained after trimming, the number of mapped reads, and the total mapping rate (%). All samples exhibit high mapping rates (>98%), confirming the high quality of the RNA-seq libraries and the reliability of gene expression quantification in hybrid and parental genotypes.

Samples	Sequence pairs	Number of paired-end alignments with a unique best hit	Mapping Efficiency (%)	Duplication Rate (%)	Deduplicated Leftover Sequences	Genome Size (Mb)	Average Depth (X)
Hyb_C.aus_rep1	59471997	45299369	76.2	21.17	35707603	359	25.56
Hyb_C.aus_rep2	56997431	43090193	75.6	23.2	33092958	359	24.5
Hyb_C.aus_rep3	52490561	40235003	76.7	22.88	31029064	359	22.56
Hyb_C.ret_rep1	59471997	44722620	75.2	21.75	34997498	349	25.56
Hyb_C.ret_rep2	56997431	42539674	74.6	23.69	32461335	349	24.5
Hyb_C.ret_rep3	52490561	39753625	75.7	23.55	30389785	349	22.56
*C. reticulata*_rep1	54120503	43591838	80.5	23.67	33274917	349	23.96
*C. reticulata*_rep2	53416001	41156597	77.0	22.69	31818808	349	22.82
*C. reticulata*_rep3	50019636	38564496	77.1	18.48	31436564	349	22.67
*C. australasica*_rep1	53564928	41617819	77.7	26.86	30441058	359	21.67
*C. australasica*_rep2	54127489	41896425	77.4	26.90	30627038	359	21.81
*C. australasica*_rep3	53798201	41649738	77.4	25.70	30946374	359	21.97

Table S2. Mapping statistics of WGBS data for hybrid and parental samples.

For each biological replicate, the table reports the number of paired-end reads obtained, the number of uniquely aligned pairs, the mapping efficiency (%), the duplication rate (%), the number of deduplicated reads, the estimated genome size used for mapping (in megabases), and the average sequencing depth (X). The samples include the hybrid mapped to both parental haplotypes (Hyb_C.ret and Hyb_C.aus), as well as the two parental species (C. reticulata and C. australasica).

Orientation	Targeted region / Primer name	primer sequence	experiment
For	Fortune_hyb_Chr01:1834900-1835400(-)CITRE_001g000830	AATYAAATTTYTYGAGAGTGAAGAGAAG	BS-PCR
Rev	Fortune_hyb_Chr01:1834900-1835400(-)CITRE_001g000830	CRTCATTRAATTCTCTRTTACATRAATT	BS-PCR
For	Aus_hyb_Chr02:25606838-25607338(-)CITRE_001g010040	YATTTATTTCTYTYTTAAGTTAAAGAGGTGATT	BS-PCR
Rev	Aus_hyb_Chr02:25606838-25607338(-)CITRE_001g010040	TARTCTCATCCACRARRATTTTRTAAAT	BS-PCR
For	Aus_hyb_Chr05:598460-598960(+)CITRE_005g025730	ACTTYYATYGTTTGYTYAAATGGYGG	BS-PCR
Rev	Aus_hyb_Chr05:598460-598960(+)CITRE_005g025730	AACCARTAAAAATRACAAARATACCCAAA	BS-PCR
For	Aus_hyb_Chr02:39307299-39307799(+)CITRE_008g010520	ATGGTAYTTGTGYACAAAAATGGGG	BS-PCR
Rev	Aus_hyb_Chr02:39307299-39307799(+)CITRE_008g010520	TARTCTTTACACCCATTACCRCAAAARAA	BS-PCR
For	Fortune_hyb_Chr06:15304575-15305075(+)CITRE_001g028710	ATATTTTGAGTGYGGGTYYGGTAYGGG	BS-PCR
Rev	Fortune_hyb_Chr06:15304575-15305075(+)CITRE_001g028710	CAARCARTTTCATCAACRATATTTTCAA	BS-PCR
For	1g001500a_F	AGCATTCAGCAAATCTAGCTAGG	RT-qPCR
Rev	1g001500ab_R	GTGACATCCGATCTCAGTTGTC	RT-qPCR
For	1g001500b_F	CAGCATTCAGCAAATCTAGCTAGT	RT-qPCR
For	2g020080b_F	TACATATTTATCCTGGCAGTGCA	RT-qPCR
Rev	2g020080b_R	CCACGCCAGCTCAACTGCG	RT-qPCR
For	2g020080a_F	TACATATTTATCCTGGCAGTGCG	RT-qPCR
Rev	2g020080a_R	CCACGCCAGCTCAACTGCA	RT-qPCR
For	2g038700a_F	CATGCGTAAAACCGGGAGAC	RT-qPCR
Rev	2g038700a_R	CAGTGTCCCAACCGTAGTCA	RT-qPCR
For	2g038700b_F	CATGCGTAAAACCGGGAGCA	RT-qPCR
Rev	2g038700b_R	CTGTGTCCCAACCGTAGTCG	RT-qPCR
For	3g001830a_F	CCAATACACGACCGCTGGAC	RT-qPCR
Rev	3g001830a_R	GGGCTTACCCGTGTTGTAGT	RT-qPCR
For	3g001830b_F	CCAATACACGACCGCTGGAA	RT-qPCR
Rev	3g001830b_R	GGGCTTACCCGTGTTGTAGC	RT-qPCR
For	3g047040a_F	AAGCACAAGGGAGAGCACCAG	RT-qPCR
Rev	3g047040a_R	GGTGAACATCAGTAGTGCCGG	RT-qPCR
For	3g047040b_F	AAGCACAAGGGTGAGCACCAT	RT-qPCR
Rev	3g047040b_R	ATGGTGAACATCAGTAGTACCGA	RT-qPCR

Table S3. List and sequences of the primer used in this study.